Atmos. Chem. Phys. Discuss., 12, 23135–23193, 2012
www.atmos-chem-phys-discuss.net/12/23135/2012/
doi:10.5194/acpd-12-23135-2012

Atmospheric Chemistry and Physics Discussions

35 years of stratospheric aerosol measurements at Garmisch-Partenkirchen: from Fuego to Eyjafjallajökull, and beyond

T. Trickl, H. Giehl, H. Jäger, and H. Vogelmann

Karlsruher Institut für Technologie, Institut für Meteorologie und Klimaforschung (IMK-IFU), Kreuzeckbahnstr. 19, 82467 Garmisch-Partenkirchen, Germany

Received: 23 July 2012 – Accepted: 18 August 2012 – Published: 6 September 2012

Correspondence to: T. Trickl (thomas.trickl@kit.edu)

Published by Copernicus Publications on behalf of the European Geosciences Union.

Abstract

The powerful backscatter lidar at Garmisch-Partenkirchen (Germany) has almost continually delivered backscatter coefficients of the stratospheric aerosol since 1976. The time series is dominated by signals from the particles injected into or formed in the stratosphere due to major volcanic eruptions, in particular those of El Chichon (Mexico, 1982) and Mt. Pinatubo (Philippines, 1991). The volcanic aerosol disappears within about five years, the removal from the stratosphere being modulated by the phase of the quasi-biennial oscillation. Here, we focus more on the long-lasting background period since the late 1990s and 2006, in view of processes maintaining a residual lower-stratospheric aerosol layer in absence of major eruptions, as well as the period of moderate volcanic impact afterwards. During the long background period the stratospheric backscatter coefficients reached a level even below that observed in the late 1970s. This suggests that the predicted potential influence of the strongly growing air traffic on the stratospheric aerosol loading is very low. Some correlation may be found with single strong forest-fire events, but the average influence of biomass burning seems to be quite limited. No positive trend in background aerosol can be resolved over a period as long as that observed by lidar at Mauna Loa or Boulder. This suggests being careful with invoking Asian air pollution as the main source as found in the literature. Rather an impact of previously missed volcanic eruptions on the stratospheric aerosol must be taken into consideration. A key observation in this regard was that of the plume from the Icelandic volcano Eyjafjallajökull above Garmisch-Partenkirchen (April 2010) due to the proximity of that source. The top altitude of the ash next to the source was reported just as roughly 9.3 km, but the lidar measurements revealed enhanced stratospheric aerosol up to 14.5 km. Our analysis suggests for two, perhaps three, of the four measurement days the presence of a stratospheric contribution from Iceland related to quasi-horizontal transport, contrasting the strongly descending lower layers entering Central Europe. The backscatter coefficients within the first 2 km above the tropopause exceed the stratospheric background by a factor of three to four. In

ACPD

12, 23135–23193, 2012

addition, Asian and Saharan dust layers were identified in the free troposphere, Asian dust most likely even in the stratosphere. The number of minor mid-latitude eruptions has gradually increased during the past ten years. We conclude that, although their stratospheric contribution could not be clearly identified above our site they can sum up for forming some minor background. Clear stratospheric signatures were only seen in the case of eruptions reaching higher altitudes.

1 Introduction

The stratospheric aerosol layer continues to attract research activities because of its (varying) impact on radiation (e.g., Charlson et al., 1991; Hansen et al., 1997; Robock, 2000; Solomon et al., 2011) and air chemistry, in particular ozone depletion (e.g., Pittock, 1965; Grams and Fiocco, 1967; Jäger and Wege, 1990; Solomon et al., 1996; Solomon, 1999). Research is needed to elucidate further the different sources, in particular those for which a positive trend is expected. Bigg (1956) concluded a potential tropospheric source of the stratospheric particles from meteorological correlations, in contrast to an also discussed cosmic origin. The detection of the mainly sulphuric nature of stratospheric aerosol (Junge and Manson, 1961; see also Berresheim and Jaeschke, 1983) then gave a strong hint on its principal relation to strong volcanic eruptions. With the advent of laser sounding this layer could be sensitively detected (Fiocco and Grams, 1964) and the time series obtained, since 1972, by lidar, balloon ascents and also satellite observations (for recent reviews see Deshler et al., 2006; Deshler, 2008), covering a number of important eruptions, have led to a clear evidence of the mainly volcanic nature of the stratospheric aerosol. Secondary sources could be strong injections from biomass burning (e.g., Fromm and Servranckx, 2003; Fromm et al., 2000, 2008a, b, 2010), likely to become more important in a warmer climate, or emissions by air traffic. Also the potential influence of the growing Asian SO_2 emissions from coal burning has been discussed (Hofmann et al., 2009).

ACPD
12, 23135–23193, 2012

In 1973, a powerful backscatter lidar was installed in Garmisch-Partenkirchen (Germany). This system yielded routine measurements of tropospheric backscatter profiles over a long period of time (Reiter and Carnuth, 1975; W. Carnuth, unpublished results). After adding single-photon counting to the analogue detection in 1976 the measurements were extended into the stratosphere. The stratospheric series has been carried on until now with short interruptions mainly caused by technical problems. A scientific summary for the period 1976–1999 was given by Jäger (2005). Deshler et al. (2006) and Deshler (2008) compared the results for the most important stations performing stratospheric aerosol sounding.

In 1991 the system was integrated into the Network for the Detection of Stratospheric Change (NDSC, now: NDACC, Network for the Detection of Atmospheric Composition Change). Since 1998 the lidar has also contributed to the German Lidar Network (Bösenberg et al., 2001) and later the European Aerosol Research Lidar Network (EARLINET; Bösenberg, 2003).

During the past, the volcanic signatures observed with the lidar have been caused by eruptions in rather remote parts of the world. A new situation arose with the eruption of the Icelandic volcano Eyjafjallajökull in April 2010, a source substantially closer to the observational site in Central Europe. The advection to Garmisch-Partenkirchen was direct due to an anti-cyclonic flow pattern, and additional stratospheric aerosol was observed. However, the top altitude of the ash cloud reached over the volcano is reported as "> 8 km" (Massie, 2012) during the first phase which could be too low for injections into the stratosphere. On the other hand, given the low tropopause in Arctic spring it has been reasonable to assume that some hot gas carrying finer particles or leading to formation of aerosol has ascended beyond the reported ash plume and reached the lower stratosphere, which could explain our observations.

This eruption was important also because of the proximity to the European Aerosol Research Lidar Network (EARLINET), Garmisch-Partenkirchen being a rural station of that network pretty much in its centre. After the first warning at noon on 15 April 2010, co-ordinated measurements have been performed during the two eruption periods in

ACPD
12, 23135–23193, 2012

April and May 2010, that reached rather different parts of Europe demonstrating the importance of such a lidar network, in particular in view of the shutdown of European air traffic over many days. In addition, extensive aircraft-based measurements have been made (Schumann et al., 2011). The observations have led to studies of the spatial propagation of the plume (Ansmann et al., 2010; Flentje et al., 2010; Schumann et al., 2011; Dacre et al., 2011; Emeis et al., 2011; Gasteiger et al., 2011; Mona et al., 2012; Pappalardo et al., 2012; Rauthe-Schöch et al., 2012), microphysical properties (Ansmann et al., 2010, 2011; Gasteiger et al., 2011; Seyfert et al., 2011; Groß et al., 2012; Mona et al., 2012) and ice formation (Hoyle et al., 2011; Seyfert et al., 2011; Steinke et al., 2011; Bingener et al., 2012). Estimates of aerosol mass have been attempted (Ansmann et al., 2011; Gasteiger et al., 2011). The conversion of optical coefficients into mass can be made with a relative uncertainty of less than 20 % with the exception of fresh volcanic plumes containing particles with radii of more than 15 µm (Ansmann et al., 2011). This approach can, therefore, be used for decisions on air traffic.

In this paper, we give a brief overview of previous findings during the 35 years of measurements at Garmisch-Partenkirchen. However, the focus here is on the long background period after 1997 and the processes determining the residual stratospheric aerosol under these conditions. The following volcanic period is used for examining the impact of small and moderate eruptions. Due to its proximity to our site the Eyjafjallajökull eruption in April 2010, that just touched the tropopause, was expected to yield relevant information on the potential stratospheric impact of an event of that magnitude. A detailed presentation of our results for the Eyjafjallajökull eruption, including also the troposphere, is given in Sect. 4.

2 Lidar systems

In this study we use data from measurements with two lidar systems at IMK-IFU (until 2001 IFU, i.e., Institut für Atmosphärische Umweltforschung of the Fraunhofer Society; 47°28′37″ N, 11°3′52″ E, 730 m a.s.l.) and at the nearby high-altitude station

ACPD
12, 23135–23193, 2012

Schneefernerhaus (47° 25′00″ N, 10° 58′46″ E, 2675 m a.s.l.) on the south side of Mt. Zugspitze (2962 m a.s.l.), about 6.5 km to the south-west of IMK-IFU. The lidar system at IMK-IFU is an instrument of both NDACC and EARLINET. This system was originally built in 1973 (Impulsphysik G.m.b.H.), based on a ruby laser, and, in addition to a large number of routine and campaign-type tropospheric measurements (e.g., Reiter and Carnuth, 1975; Jäger et al., 1988, 2006; Forster et al., 2001; Trickl et al., 2003, 2011), has been almost continually used for measurements of stratospheric aerosol since autumn 1976 (e.g., Jäger, 2005; Deshler et al., 2006; Fromm et al., 2008, 2010). The lidar was converted to a spatially scanning system with a Nd:YAG laser (Quanta Ray, GCR 4, 10 Hz repetition rate, about 700 mJ per pulse at 532 nm) in the early 1990s for additional investigation of contrails (Freudenthaler, 2000; Freudenthaler et al., 1994, 1995) and, for the routine measurements, has been operated at the wavelength of 532 nm ever since. The stratospheric measurements discussed here have taken place during nighttime (vertical pointing, range: 2 km a.s.l. to more than 40 km a.s.l.) because of the necessity of single-photon counting and of reducing background signals. The vertical bins of this 300-MHz multichannel scaler (FAST ComTec) are 75 m wide. Four subsequent measurements are made without attenuation and with three different attenuators, the strongest one being used for the near-field detection. A high-speed chopper is used to cut off the strongest part of the signal. For each attenuation step a different chopper delay is applied (minimum distance achieved: 1.3 km). In the NDACC data base, following the format prescription, the data are not smoothed which in the case of strong extinction can lead to noise spikes in the lowest data segment within the tropopause region. With this lidar system rather small aerosol structures exceeding roughly 2 % of the Rayleigh return at 532 nm (that corresponds to a visual range of more than 400 km above 3 km) can be resolved within the free troposphere.

The backscatter coefficients have been calculated by iterative solution of the lidar equation. They are carefully adjusted to match the Rayleigh backscatter coefficients at long distances. In this procedure the atmospheric density is obtained from the routine radiosonde ascents at Oberschleißheim (“Munich radiosonde”, sta-

ACPD
12, 23135–23193, 2012

tion number 10868) and by using NCEP (National Centers for Environmental Prediction) data for the higher altitudes. The backscatter signals have been corrected for the light absorption by ozone in the stratosphere cross section for both the ruby wavelength and the wavelength of the frequency-doubled Nd:YAG laser (Brion et al., 1998; http://igaco-o3.fmi.fi/ACSO/cross_sections.html). Climatological seasonally varying ozone profiles have been taken, obtained from the nearby Meteorological Observatory Hohenpeißenberg of the German Weather Service. The Rayleigh backscatter coefficients have been calculated from the very accurate algorithm provided by Owens (1967) and King factors obtained from a least-squares fit to the wavelength-dependent data by Bates (1984). The aerosol backscatter coefficients can be calculated with a relative uncertainty of 10 to 20 % under optimum conditions.

A number of aerosol measurements have been contributed by the water-vapour differential-absorption lidar (DIAL), operated at the Schneefernerhaus high-altitude research station. The full details of this lidar system were described by Vogelmann and Trickl (2008). This lidar system is based on a powerful tunable narrow-band Ti:sapphire laser system with up to 250 mJ (typically used: 100 mJ) energy per pulse operated at about 817 nm and a 0.65-m-diameter Newtonian receiver. Due to these specifications a vertical range up to about 12 km is achieved, almost independent of time during the day, with measurement durations of about fifteen minutes. The vertical resolution chosen in the data evaluation is dynamically varied between 50 m in altitude regions with good signal-to-noise ratio and roughly 250 m in the upper troposphere. The noise limit above 10 km a.s.l. corresponds to about 1.5×10^{20} m^{-3} (density) or about 18 ppm (mixing ratio). Free-tropospheric measurements during dry conditions clearly benefit from the elevated site outside or just below the edge of the moist Alpine boundary layer (e.g., Carnuth and Trickl, 2000; Carnuth et al., 2002). After extensive testing, validating and optimizing the system, routine measurements were started in January 2007 with typically two measurement days per week, provided that the weather conditions are favourable. During this period also successful comparisons with an air-borne DIAL and

ACPD
12, 23135–23193, 2012

a ground-based Fourier-transform infrared spectrometer were achieved verifying the absence of a bias exceeding 1 % (Wirth et al., 2009; Vogelmann et al., 2011).

The 817-nm measurements yielded additional information on the aerosol backscatter coefficients during a shut-down period of the NDACC lidar from May to September 2009 and during some day-time period on 19 April 2010. Due to its power and its large receiver this system has a rather wide range in the "off" wavelength channel reaching far into the stratosphere. However, since analogue data acquisition is used the signal quality starts to deteriorate in the far field due to electromagnetic interference and amplification noise. In particular, a small interference by the magnetic field caused by the flashlamp current of the Nd:YAG pump laser (Trickl, 2010) persists. This broad feature, lasting for several hundred microseconds, was determined from dark measurements, numerically smoothed and subtracted from the data, which resulted in noise-limited backscatter signals.

For the period in 2009 the 817.22-nm-data with the best signal-to-noise ratio were taken. The Fernald-Klett method was applied (Fernald, 1984; Klett, 1985). The reference values were adjusted to yield optimum results at lower altitudes, e.g., in ranges without discernible aerosol which was possible in several cases. In addition, the results from different measurements were verified to agree in altitude ranges without structures from fresh plumes. Due to the lower level of Rayleigh backscattering, the calibration of the aerosol backscatter coefficients is a more demanding task than at 532 nm, and was done with particular care. The backscatter-to-extinction ratio was chosen as $0.02\,\mathrm{sr}^{-1}$ which is the climatological mean value found within EARLINET (e.g., Mattis et al., 2004). The data were converted to 532.26 nm by assuming a $\lambda^{-1.4}$ wavelength dependence (Jäger and Deshler, 2002, 2003) and then averaged within the standard 75-m vertical bins of the aerosol lidar. For the conversion of the Rayleigh backscatter coefficient a factor of 5.9605 was used, again derived from the algorithm by Owens (1967) and the data by Bates (1984). Because of narrowband filtering of the DIAL return just the contribution of Raman Q branch was included, calculated from the King factor. The influence of ozone was neglected since

ACPD
12, 23135–23193, 2012

the absorption cross section at 817 nm is 1/12 of that at 532 nm (Brion et al., 1998; http://igaco-o3.fmi.fi/ACSO/cross_sections.html).The final treatment was done with the standard procedure for the NDACC lidar, including the conversion to 694 nm traditionally performed for the integrated backscatter coefficients. The results for 532 nm were compared with those of the NDACC lidar within the neighbouring periods as an addition quality control.

We frequently use the scattering ratio,

$$R = \frac{\beta_R + \beta_P}{\beta_R}, \quad (1)$$

with the Rayleigh and particle backscatter coefficients β_R and β_P, respectively. Due to its normalization to the Rayleigh backscatter coefficients the scattering ratio gives a better idea of the "optical impact". Like a mixing ratio it also is independent of the air number density. On the other hand the normalization by β_R (which is proportional to the air density) amplifies the noise of the data towards higher altitudes. Here, the high sensitivity of the big aerosol lidar is important.

3 Results for the period 1976–2009

The most recent version of the Garmisch-Partenkirchen time series of the integrated backscatter coefficient is shown in Fig. 1. The backscatter coefficients are integrated from 1 km above the tropopause (thermal tropopause of the midnight Munich radiosonde ascents, 100 km roughly to the north). The series is displayed here without errors for clearness. The errors were specified (for the shorter period until 1999) in the preceding publication by Jäger (2005). In the following we describe some of the characteristics of different time periods.

ACPD
12, 23135–23193, 2012

3.1 Results 1976–1996

The time series is dominated by signals from the particles injected into the stratosphere by major volcanic eruptions, in particular those of El Chichon (Mexico, 1982) and Mt. Pinatubo (Philippines, June 1991). The first volcanic aerosol peak in the stratosphere above Garmisch-Partenkirchen was that of Fuego (Guatemala, October 1974), observed during test measurements on 10 January 1975 (Reiter et al., 1979). This observation was made just with an oscilloscope, prior to the installation of adequate lidar detection electronics and could, thus, not be evaluated quantitatively. As pointed out by Deshler (2008) this eruption, together with other, minor eruptions, influenced the aerosol level during the quasi-background period before 1980, and, thus, our earliest measurements taken into consideration for our series in autumn 1976. Other data suggest a much lower background for the period before 1974. The reason is not clear. There had been a long rather silent period after 1910, but in 1963 there was a significant eruption of Mt. Agung (Bali, Indonesia) that should have modified the background (e.g., Robock and Free, 1995; Robock, 2000).

The volcanic aerosol after the El-Chichon and Pinatubo peaks disappeared within about five years, the removal from the stratosphere being modulated in phase with the quasi-biennial oscillation (Jäger, 2005).

3.2 Results 1997–2006

During the background phase starting in 1997 the aerosol loading of the stratosphere was rather low (Fig. 1) and exhibited only very short elevated-aerosol events. Some of these events are discussed in the following section. On some days it was even difficult to resolve any aerosol component in the lidar signals received from the stratosphere. As during the volcanic periods a pronounced seasonal cycle is seen, caused by, e.g., the seasonal variation of the tropopause height or vertical exchange across the tropopause.

ACPD
12, 23135–23193, 2012

Starting in 2004, a slight increase of the background aerosol is indicated. In late 2006 this increase is accelerated by the beginning of a new volcanic period. Therefore, we evaluated the slope just during the background phase between 4 February 2004 and 21 September 2006. A linear least-squares fit (Trickl and Wanner, 1983, 1984) to the integrated backscatter coefficients (Fig. 2) and found a slope of $+2.11 \times 10^{-6}\,\mathrm{sr}^{-1}\,\mathrm{a}^{-1}$ with a relative standard deviation of 77 %. This corresponds to a rate of $+5.46\,\%\,\mathrm{a}^{-1}$, if calculated for the centre of that period. The period for which this evaluation could be made is too short for reaching reasonable statistical significance.

Nevertheless, this result is not too far from the increase reported by Hofmann et al. (2009) for the stations Mauna Loa and Boulder. The positive trend for the period 2000 to 2009 at Mauna Loa is 3.3 % for the stratospheric column and 4 to 7 % per year for the altitude range 20–30 km which is within the lower stratosphere at that low latitude. The authors ascribe this increase to the growing emissions of sulphur dioxide from coal burning, mainly in China, exhibiting a pronounced rise since 2000.

If there is a rise in our data it cannot have started before 2003 as can be estimated from extrapolating the descending values for the late post-Pinatubo phase and the values for the period after 2004. This delay with respect to the start of the rise at Mauna Loa is significant and strongly exceeds the typical half-a-year delay in the El Chichon and Pinatubo cases caused by the transport from the (sub)tropics to the mid-latitudes. If a continually emitting large-scale source such as Chinese air pollution yields a contribution one would expect a contribution also at our latitudes, but with short delay with respect to the Mauna Loa findings.

A more reasonable explanation can be derived from analysing the number of volcanic eruptions in the two latitude ranges listed by Massie (2012). These extensive listings, starting in 2004, clearly show that the number of volcanic eruptions had been strongly underestimated. In Fig. 3 one can see the impressive number of eruption periods even for limiting the plume altitudes to at least 5 km. In the tropics where we also give a curve for the additional altitude range above 15 km that should have the strongest impact on

ACPD
12, 23135–23193, 2012

the stratosphere. Table 1 lists the most significant eruptions at higher latitudes since 2000 that should have had more direct influence on our observations.

It is obvious that the number of mid-latitude eruptions stays low until 2005 and rises afterwards, in qualitative agreement with the time series in Fig. 1. By contrast, the number of eruptions between 20° S and 20° N exhibits a very strong increase in the early phase, in agreement with the earlier start of the increase of the backscatter coefficients above Mauna Loa and Boulder. The number of eruptions in this latitude range is impressive, with most contributions from South and Central America (in particular the enormously active volcano Tungurahua, 5016 m a.s.l., Ecuador, 1999 until present; http://de.wikipedia.org/wiki/Tungurahua), and Indonesia. The absence of significant volcanic eruptions during the background phase stated by Hofmann et al. (2009) is clearly not confirmed. It is, therefore, reasonable to discuss a volcanic impact on the stratosphere above the low-latitude stations.

The number of eruptions in the Southern Hemisphere south of −20° has been comparatively small. Only four eruptions have reached altitudes beyond 10 km, the most important one being that of Chaiten (Chile, 42.83° S, starting on 2 May 2008) with a top plume altitude of 30 km.

3.3 Influence of fires

During the period covered by our measurements there were three periods with low to moderate volcanic influence in the stratosphere. In the longest period of this kind, the background period since the late 1990s the influence of less important sources of stratospheric aerosol can be distinguished. One important source could be strong forest fires, a topic with growing importance on a way to a drier climate. In fact, the area burnt per year in the United States (US) has roughly doubled since the 1990s (Fig. 4).

In particular, so-called pyro-cumulonibus (pyroCb) clouds reach the stratosphere and give rise to aerosol observations above the tropopause. Two pyroCb events that yielded also plume observations at Garmisch-Partenkirchen were recently studied in an international co-operation (Fromm et al., 2008b, 2010). The first is the

ACPD
12, 23135–23193, 2012

Chisholm fire, initiating a huge burst of smoke that occurred over Northern Canada on 28 May 2001. The intense plume could be followed with TOMS satellite images (http://toms.gsfc.nasa.gov/aerosols/aerosols.html) all the way across the North Atlantic. However, it missed Garmisch-Partenkirchen during the first approach. The plume was observed with some delay during the second half of June and in early July (before a longer interruption of the measurements due to a field campaign). The source region was verified by a three-week backward simulation with the FLEXPART tracer model (N. Spichtinger-Rakowsky, personal communication, 2006). Quite interestingly, a slight positive correlation of the aerosol and the temperature in the profiles of the nearest radiosounding station, Oberschleißheim ("Munich"), 100 km roughly to the north, was found (see also de Laat et al., 2012). The Chisholm particles gradually filled the lowermost stratosphere in the entire Northern Hemisphere, as determined from observations with satellites and with NDACC lidar systems (Fromm et al., 2008b).

Even this spectacular event did not lead to more than a doubling of the integrated stratospheric backscatter coefficient after spreading over a large area in the Northern Hemisphere. These events are confined to periods of a few months. The impact of forest fires is discernible during longer background periods, but the contribution is small in comparison with that of major volcanic eruptions. The open question is: Will this contribution grow in the future?

The situation was different for the second pyroCb event studied in detail that took place in the Québec province (Canada) in June 1991 (Fromm et al., 2010). The plume was observed directly after the first passage across the Atlantic and, therefore, yielded much more pronounced signatures in the lower stratosphere. Measurements were made with both the NDACC lidar (during the first night hour of 1 July 1991) and the IFU tropospheric ozone lidar (extended time series between 1 and 3 July; see also Carnuth et al., 2002). The maximum backscatter coefficient at 313 nm was as high as $8.4 \times 10^{-6}\,m^{-1}\,sr^{-1}$, at 15 km. This corresponds to an aerosol-related horizontal visual range at 313 nm of roughly 9.3 km.

ACPD
12, 23135–23193, 2012

The lower-stratospheric plume had been initially misinterpreted as the first arrival of Mt. Pinatubo aerosol over Garmisch-Partenkirchen. We calculated a total of 111 315-h HYSPLIT (Draxler and Hess, 1998; http://ready.arl.noaa.gov/HYSPLIT_traj.php) backward trajectories for this episode, at intervals of three hours, starting at altitudes between 13.5 and 16 km over Garmisch-Partenkirchen. Trajectories from the two relatively strong lower-stratospheric plumes (Fig. 6 of Fromm et al., 2010) overpass the region around Québec City where the fires took place. All the other trajectories end in regions ranging from the subtropical Atlantic Ocean to Central America and the US, or over the Eastern Pacific Ocean. There is almost no chance of significant overlap with the Pinatubo eruption on 13 June 1991.

3.4 Polar stratospheric clouds

Polar stratospheric clouds (PSCs) are normally observed in the Arctic regions. However, the Arctic polar vortex sometimes stretches to mid-latitudes and PSCs have been occasionally observed as far south as Southern France (Keckhut et al., 2007). Over Garmisch-Partenkirchen (lidar: 47.477° N) PSC events were observed on 5 March 1996 (see remarks by Keckhut et al., 2007), a thin peak at 19.9 km and on 19 February 2008 (Figs. 5, 6). The Munich radiosonde reveals pronounced temperature troughs between 19 and 23 km in both cases. The minimum temperatures registered next to (i.e., vertical distance less than 3 km) the PSCs were −80.3 °C and −83.7 °C, respectively. 315-h HYSPLIT backward trajectories, initiated above our lidar site in the evening of both days, reveal horizontal advection of that layer from the polar region via Greenland and the UK, after rapidly circulating around the North Pole several times (not shown). For the March-1996 case the trajectories stay at high latitudes whereas in the February-2008 case they follow some elongated pattern between Canada and Siberia.

ACPD
12, 23135–23193, 2012

3.5 Revival of volcanic activity in recent years

An interesting temporary aerosol event was observed in December 2006 (Fig. 7), within a first significant rise of the integrated backscatter coefficient in Fig. 1 after the long background period. Up to 30 km or more, the stratosphere was loaded with aerosols for a few days. No major volcanic eruption or wild fires could be identified during the two months preceding these observations. Significant mid-latitude eruptions were missing since 9 May (Bezymianny, Kamtchatka; top of plume: 15 km; see Table 1).

Since very cold temperatures prevailed in the stratosphere from Novaya Semlya to the Alps and, further to the east, to Northern Greece, one could think about a vertically extended PSC. However, the Munich radiosonde showed minimum temperatures of just −70 °C (12 to 25 km a.s.l.), not enough for PSC formation. Also the calculated HYSPLIT 315-h backward trajectories did not reach regions with temperatures below −80 °C.

We now tend to believe that a highly delayed arrival of the eruption plume from the Soufrière Hills volcano (Caribbean Sea; 20 May 2006), which reached 16.8 km (Massie, 2012) and stayed in the tropics for some time (Prata et al., 2007), can explain the observations. The entire ensemble of stratospheric HYPSLIT trajectories calculated for the measurement days in December 2006 (up to 25 km) started at low latitudes of the Northern Hemisphere during the final round. Even if the aerosols had stayed at low latitudes for many months some fraction of it could reach our site in December. Indeed, the wide distribution of particles seen in Fig. 7 suggests a considerable age of that plume.

A second possibility is the eruption of Rabaul (New Guinea) on 7 October 2006 that reached 18 km. This eruption was short, occurred in the Southern Hemisphere (4.27° S), and the plume propagated farther to the south. Thus, a contribution from there is not very likely.

During the years 2008 and 2009 several volcanic eruptions leading to observations of stratospheric aerosol were reported (Okmok, Aleutian Islands; Kasatochi, Alaska,

ACPD
12, 23135–23193, 2012

7–8 August; Redoubt, Alaska; Sarychev, Kuril Islands; see Table 1) (Massie, 2012; Martinsson et al., 2009; Bourassa et al., 2010; Heue et al., 2010; Mattis et al., 2010; Kravitz et al., 2011; Campbell et al., 2012). These plumes resulted in rather confined layers, observed at several European lidar stations.

Due to a major field campaign and subsequent construction work at IMK-IFU the stratospheric lidar measurements had to be interrupted between 6 May and 29 September 2009. Because of the strong eruptions occurring in spring 2009 we filled this gap with the data from Zugspitze DIAL system (Sect. 2.1). In Figs. 8 and 9 we give a few examples from May to September 2009. The scattering ratios (not shown) outside narrow structures, converted to 532 nm, grew from 1.1 to 1.4 during that period in agreement with the results of the NDACC lidar before and after the gap.

Between 5 May and 30 June 2009, some spikes were detected between the tropopause and about 14 km (532-nm scattering ratio $R \leq 1.4$). This structure was tentatively assigned to the Redoubt eruption, HYSLPIT giving clear evidence just on 26 May. This structure disappeared before 14 July.

The Sarychev plume was first observed on 14 July and exhibited several thin layers between 14 km and 19 km ($R \leq 2.2$). A separate spike next to 22 km ($R = 2.5$ on 16 July) was observed both on 14 and 16 July. During the first months a pronounced intraday variability of the structure was observed. The highest values ($R \approx 2.4$, $\beta_P \approx 3 \times 10^{-7}\,m^{-1}\,sr^{-1}$ at about 17 km) occurred by the end of July and in August. Towards the end of September 2009 a transition to a smoother distribution occurred that continued to be present into the following year. The top 532-nm scattering ratio extended to more than 1.4 ($\beta_P \approx 1 \times 10^{-7}\,m^{-1}\,sr^{-1}$ at about 16 km) by the end of September 2009 and gradually diminished to 1.15 in February 2010, about 1.1 in April and 1.07 in July. During this period the layer widened to a plateau that extended to 28 km by the end of June 2010, the aerosol layer ending at 30 km, and then gradually shrinked in vertical extent. The behaviour qualitatively agrees with that for 1064 nm reported by Mattis et al. (2010) for Leipzig during the period 2008–2009. However, the infrared values seem to be rather low which indicates small particles (one August example for

ACPD
12, 23135–23193, 2012

532 nm being in relatively good agreement with our results). Indeed, Mattis et al. (2010) derived an effective radius of 0.2 µm and Ångström coefficients up to 2.

The top altitude of the Sarychev eruption is listed in the "Summary of volcanic activity" (Massie, 2012) as just 10 km (Table 1) in clear disagreement with our observations. Kravitz et al. (2011) quote a much higher altitude of 16 km (the "mushroom" in their Fig. 1, taken from space, is impressive), and sources on the internet suggest much higher altitudes up to 18 km. In order to verify this we analysed aerosol images from the space-borne lidar CALIOP (Cloud-Aerosol LIdar with Orthogonal Polarization) onboard the CALIPSO (Cloud-Aerosol Lidar and Infrared Pathfinder Satellite Observation) satellite for an extended period of time (http://www-calipso.larc.nasa.gov/). A westward component was observed at altitudes up to 23.5 km over East Siberia, the westward plume was found between 15 and 18 km south of Alaska and later over Western North America. In contrast to the Eyjafjallajökull plume described in the following section the Sarychev aerosols were not depolarizing which indicates spherical particles in some agreement with the idea of a condensation of SO_2 as an important aerosol source (Kravitz et al., 2011).

4 Eyjafjallajökull 2010, and beyond

The Icelandic Volcano Eyjafjallajökull started to erupt on 14 April 2010. Within an anticyclonic air stream the ash plume headed for Central Europe, a unique target for coordinated lidar sounding by EARLINET. The EARLINET stations were independently warned by us and the EARLINET team in Potenza in the early afternoon of 15 April well before the ash plume reached the coast of the North Sea on Friday, 16 April, and the Alps on Saturday, 17 April (Fig. 10). Propagation further southward was prohibited by a low-pressure zone over Northern Italy during the first approach. Thus, Garmisch-Partenkirchen was the southernmost EARLINET station detecting the direct ash plume during the first approach.

ACPD
12, 23135–23193, 2012

The anti-cyclonic descent was, slightly before the eruption, accompanied by a stratospheric air intrusion starting over Greenland and Iceland, forecasted by the daily operational four-day trajectory forecasts by ETH Zürich (e.g., Zanis et al., 2003; Trickl et al., 2010) and documenting the vicinity of the jet stream. Indeed, the subsidence observed at Leipzig, Maisach and Hohenpeißenberg (Ansmann et al., 2010; Flentje et al., 2010) resembled that mostly observed for stratospheric air intrusions in our area (e.g., Eisele et al., 1999; Zanis et al., 2003; Trickl et al., 2010). The intrusion did not penetrate Central Europe much since the anti-cyclone was located to its north-west. During the second period in May, again, anti-cyclonic conditions prevailed, and a stratospheric intrusion descended from Northern Greenland to Spain for several days.

For several days, ash reached the Northern rim of the Alps. The detection with the lidar systems at Garmisch-Partenkirchen, in contrast to those at Hohenpeißenberg (38 km to the north; Flentje et al., 2010) and Maisach next to Munich (Ansmann et al., 2010; Gasteiger et al., 2011), was impeded by frequent clouds and, in part, rain due to repetitive low pressure over Italy or convective conditions. The only exception was 19 April, when clear conditions prevailed and also made possible daytime measurements with the water-vapour DIAL. The arrival of the ash could not be determined visually because of a reduced visibility on and before 17 April. Also mostly because of truly bad weather conditions just a single early-night measurement with the NDACC lidar was made in May (on 9 May).

In the following subsections both the observational data and the analysis for the period between 17 and 23 April are presented. We describe the results for both the troposphere and the stratosphere. Starting on 20 April the complexity of the aerosol contributions in the entire range increased considerably, which required very detailed analyses.

4.1 Radiosonde and radar data

Table 2 shows the tropopause altitude and maximum upper-tropospheric relative humidity from the radiosonde ascents at the stations Keflavik (Iceland) and Munich

ACPD
12, 23135–23193, 2012

(100 km north of our site) for 13 to 23 April 2010 (http://weather.uwyo.edu/upperair/sounding.html). Due to the sometimes complex temperature distribution we define the tropopause as the first temperature inversion next to the final drop in relative humidity towards the stratosphere. The values stay below 10 km for the most important period between 14 and 17 April.

For 14–17 April the period of strongest eruption, the maximum relative humidity is of the order of 80 % which could foster aerosol growth, or could indicate the vicinity of even wetter layers favourable for the formation of cirrus clouds, in particular when considering the higher relative humidity over ice.

Also above Munich the tropopause was low. However, much rather drier conditions prevailed than over Iceland. In Table 2 just the highest relative humidity value in the upper troposphere is given.

The maximum eruption altitude is specified as "> 8 km" by Massie (2012). Petersen (2010) and Arason et al. (2011) display time series of the eruption altitude based on radar measurements. The highest altitude in Fig. 9 of Arason et al., 9.3 km, is given for the early afternoon of 14 April associated with the first eruption peak and slightly above the Keflavik 12:00 UTC tropopause (Sect. 4.4, Table 2). The true top value could be even slightly higher because of the radar scans were carried out for discrete elevation angles. Peak altitudes between 8.0 and 8.7 km are repeatedly marked between 16 April and early 18 April the period most important for our observations. On 18 and 19 April the peak altitude dropped, oscillating between 2 and 5 km.

The tropopause values for Keflavik are very close to the maximum altitudes reached by the eruption. The highest altitudes reached, in part, exceed the corresponding Keflavik tropopause level. Additionally, one cannot exclude that some of the hot gas from the eruption, condensing or loaded with a certain fraction of small particles, rose to 10 km and higher without being detected.

ACPD
12, 23135–23193, 2012

4.2 Observations at Garmisch-Partenkirchen

The results for all four measurement nights with the NDACC lidar are shown in Figs. 11 and 12, those for the DIAL in the late afternoon of 19 April in Fig. 13. In addition, we show in Fig. 14 a water-vapour profile obtained from the same measurements underlying Fig. 13. The main part of the ash was observed below 4 km on all days, with backscatter coefficients between 2.2×10^{-6} m^{-1} sr^{-1} and 3.4×10^{-6} m^{-1} sr^{-1} (corresponding to a visual range of the order of 30 km). This is roughly one third of the values reported for Maisach and Leipzig and one fifth of the values reported for Hamburg (Ansmann et al., 2010), in qualitative agreement with the FLEXPART results in Fig. 10 that indicate less overlap of the plume with our site.

The presence of the volcanic plume at about 3000 m is confirmed by the SO_2 measurements at the Schneefernerhaus (2650 m a.s.l.) by the German Weather Service (Flentje et al., 2010; Gilge and Plass-Dülmer, 2010). A strong rise in SO_2 is seen on 17 April after 10:00 Central European Time (CET = UTC + 1 h; first peak: 3.3 ppb at 13:30 CET), SO_2 staying high until the early morning of 18 April. The maximum in PM_{10} particles measurements at the Schneefernerhaus was reached at about 22:00 CET. Another pronounced peak occurred on 19 April around 19:00 CET, matching the measurement time of the NDACC lidar. The period of continuously elevated SO_2 ended on 20 April at about 19:00 CET. Afterwards, including 23 April, the last measurement day of the lidar, just minor SO_2 structures between 0.1 and 0.3 ppb are seen. In the evening of 23 April both a small SO_2 peak and a small aerosol peak are seen in the Schneefernerhaus data (Gilge and Plass-Dülmer, 2010). The aerosol peak at 3.25 km in the lidar measurement in Fig. 11 and the trajectories (Sect. 4.2) suggest the presence of at least some Icelandic ash slightly above the station also in this evening.

In addition to the spikes next to 3000 m we see a rugged aerosol pattern weaker by one order of magnitude also in the free troposphere. There was additional aerosol even in the lower stratosphere, on 20 April up to 14.3 km. This lower-stratospheric contribution clearly differs from the weak broad background hump in the late period of the

ACPD
12, 23135–23193, 2012

Sarychev phase that exhibited low values above the tropopause (including occasional small spikes until March) and a maximum around 18 km. Nevertheless, due to their small size the aerosol contributions above the tropopause must be interpreted with care.

As mentioned, Table 2 shows quite different humidity conditions for Keflavik and Munich. On 15 and 16 April, the upper tropospheric relative humidity (RH) over Iceland was high, touching the range favourable for aerosol growth. By contrast, low to moderate humidity prevailed in the upper tropospheric over Munich throughout our observational period. Our own measurements for 19 April (Fig. 14) show very low free-tropospheric water vapour above 3.8 km, qualitatively agreeing with the data from Munich. The 19:42-CET measurement could not be evaluated in the tropopause region because of signal overflow within an aerosol spike. Smaller spikes were also present at the other measurement times, when the humidity was low to moderate. An interpretation by cirrus clouds is, therefore, difficult although clouds could be visually observed to the south-west in the evening indicating the approaching next storm. Seyfert et al. (2011) demonstrated the presence of ash-assisted formation of cirrus clouds during several days of the first observational period (see also other related papers cited in the introduction). Thus, it cannot be excluded that the spikes observed below the tropopause during the second half of 19 April are related to the presence of ice-covered ash particles. This would also yield a hint that ash particles were present in the tropopause region on that day. The temperature between 9 km and 10 km above Munich was between −50° and −60 °C during the period of interest favourable for any kind of freezing. The cirrus formation is likely to have occurred close to the source where higher RH was registered.

The free-tropospheric and lower-stratospheric backscatter coefficients for 20 April were clearly higher than on the other days. However, this case is rather complex and, as will be shown in the following sections, is very likely related to aerosol from several sources.

ACPD
12, 23135–23193, 2012

4.3 HYSPLIT trajectories

Roughly 260 HYSPLIT trajectory plots with at least three trajectories were generated for the period 15 to 23 April, 2010. The trajectories were calculated both backward and forward in time. Trajectories starting over a single location were extended over 315 h, ensemble trajectory plots, yielding trajectory bundles, are limited to 120 h.

Backward trajectories starting above IMK-IFU covered the altitude range from 1 km to 14 km, at intervals of typically 1 km. The observations in the PBL were characterized by reduced visibility with a visual range of the order of 40 km or less, quite unusual for our clean-air site. Before the arrival of the Icelandic plume the trajectories revealed source regions over Eastern Europe, sometimes including the region north of the Black Sea where air pollution is known to exist, but also air from Scandinavia that arrived via East Germany. We have also speculated on an early pollen episode due to the early beginning of spring. After the ash arrived it also could, have contributed to the moderate visibility. The trajectories for that period occasionally also show advection from the Sahara desert.

Around 3000 m the trajectories consistently show passage over Iceland for all four measurement times. The travel times grow from 2.5 d (17 April) to 4 d (19 April), and 8 d (20 and 23 April), consistent with a slowing of the air masses with the eastward propagation of the high-pressure zone over the North Sea. For the later three measurement days some extra loop formed next to the southern part of the UK.

In the free troposphere and lower stratosphere the situation gradually changed after the first two measurement days on which Iceland was clearly identified as a source region. In particular, on 23 April the situation was entirely different since no advection from Iceland is obtained for all altitudes above 3 km. For the range 5–8 km the trajectories lead backward to Spain and the Canary Islands, between 6 and 9 km to the north-western part of the Sahara where they propagate at altitudes below 3 km. The observation of Saharan dust in the upper troposphere, though with low concentration, is rather special, with upper boundaries being typical 5 to 6 km (e.g., Jäger et al., 1988;

ACPD
12, 23135–23193, 2012

Papayannis et al., 2008). The trajectories for 11 to 14 km stay at high altitudes and also stay far south of Iceland, passing over the US and Canada. Some of them reach the East Asian deserts at low altitude which could suggest the presence of Asian dust.

One difficulty in the interpretation via trajectory calculations is related to the obvious fast subsidence of the heaviest particles revealed by the satellite measurements (Sect. 4.4). At higher altitudes lighter particles should prevail and transport modelling should become more reliable.

In addition, we found that the forward or backward trajectories initiated over exactly the same horizontal position were not able to cover the full range of potential source or target regions, respectively. This was verified by calculating HYSPLIT ensemble trajectories where a "trajectory plume" is generated by slightly varying the initial conditions, e.g., horizontally by one grid unit. These plumes are clearly advantageous, but their calculation is restricted to 120 h. We calculated ensemble trajectories both in the forward and the backward direction. The forward calculations initiated over the volcano between 8 and 11 km yielded a transition from the initial eastward propagation of the plume to a southward propagation in the late morning of 17 April. This behaviour continued until the end of our calculations at 04:00 CET on 18 April, i.e., slightly after the end of the strong eruption period. Quite surprisingly, not visible in the normal forward trajectories, a separate branch forms that first propagates towards Greenland and then returns and enters Central Europe four days after the start of the trajectories (Fig. 15). For higher altitudes the arrival over our site shifts to earlier times, but does not become fully consistent with the early-night observation time on 20 April. In addition, these trajectories mostly suggest air-mass arrival above Garmisch-Partenkirchen several kilometres below the tropopause.

By contrast, quite a few of the cyclonically approaching trajectories from ensembles initiated on 17 April between 16:00 UTC and midnight (UTC) pass over the area around Garmisch-Partenkirchen within ±4 h from the measurement on 20 April and at altitudes between 10 and 11 km. These branches travelling more southward could not be created by starting the trajectories exactly above the volcano, which resulted in rather

ACPD
12, 23135–23193, 2012

quick turns towards Russia similar to the situation in Fig. 15. This result suggests the presence of at least some volcanic aerosols above the lidar also in the evening of 20 April.

For the early-night measurements on 20 April the backward normal and ensemble trajectories reveal advection from North America and beyond. No contact to the atmosphere above Iceland is found for altitudes above 7 km, in some disagreement with the results of the forward ensemble trajectories. One example is given in Fig. 16. Between 7 and 13 km an additional branch is seen that ends in the area southwest of Hudson's Bay on 16 April, at lower altitudes. This branch turns out to be quite important and is further discussed in Sect. 4.4. Between 5.5 and 7 km, the backward trajectory ensemble shows reasonable overlap with Iceland (Fig. 17). This is the range of the largest free-tropospheric aerosol peak in Fig. 11. The travel time is short, but passes over Eyjafjallajökull at low altitudes fitting to the eruption altitudes reported for 19 April. We, therefore, conclude that the strong peak at 5.8 km was caused by Icelandic ash.

4.4 Satellite data

Aerosol images from the CALIOP space-borne lidar onboard the CALIPSO satellite have been inspected for the entire period. In contrast to the Sarychev plume (Sect. 3.5) the Eyjafjallajökull plume was strongly depolarizing, which is consistent with the lidar observations over Europe (Ansmann et al., 2011; Gasteiger et al., 2011; Groß et al., 2012).

The orbits were rarely sufficiently close to the volcano to allow us to derive a complete time series of the top altitude of the eruption. However, passes in the vicinity indicate that at least 9 km were reached in the initial phase. Some air-mass rising to 11 km on the travel towards Europe is indicated, but some uncertainty exists about this since cirrus clouds could co-exist. Quite astonishingly, there is enhanced backscatter signal up to 10 km during the two passes of the satellite on 13 April, which exactly matched the position of Eyjafjallajökull. No big eruption is reported for that day. The upper-tropospheric humidity was just moderate.

ACPD
12, 23135–23193, 2012

Very strong subsidence is indicated for the approach towards Central Europe. By contrast the trajectories reveal subsidence by 2 km or less, depending on the altitude. This behaviour indicates a pronounced gravitational component of the heaviest ash particles.

For detecting dense aerosol plumes, TOMS (Total Ozone Mapping Spectrometer, http://toms.gsfc.nasa.gov/aerosols/) aerosol images were inspected for several weeks preceding the Eyjafjallajökull eruption. One big plume was, indeed, found that emerged from the eastern part of the Gobi desert on 8 April and could be traced forward by TOMS images to the region southwest of Hudson's Bay where it arrived between 16 and 17 April. We verified this plume along this path by CALIOP images. The main portion stayed around 5 km, but also upper-tropospheric contributions were present up to roughly 8 km. In combination with trajectory results in Sect. 4.2 we conclude that the aerosol layers between 7 km and 13 km are related to a dust storm in East Asia, with potential contributions from Iceland. In fact, several of the single 315-h backward trajectories along the extended westward branch in Fig. 16 pass over the Gobi desert directly, in part next to the ground, but several days later than the plume in the TOMS image. This pathway is also shifted northward with respect to the TOMS plume over North America.

4.5 The 2011 eruptions

The new period of strong volcanic activity did not come to an end in 2011. Two more violent eruptions, those of Grimsvötn (Iceland, 21 May 2011, and Nabro, Eritrea, 12 June 2011) injected material into the stratosphere. There is consensus within the international lidar community that the pronounced rise in stratospheric aerosol in summer and autumn 2011, resulting in the characteristic violet sky after sunset, was due to the Nabro plume. Grimsvötn exploded spectacularly (Fig. 18), and the ash was, indeed, observed over Scandinavia (Tesche et al., 2012). We do not have any evidence of having detected aerosol from that plume above our site.

ACPD
12, 23135–23193, 2012

The Nabro plume reached an altitude of 13.7 km (Massie, 2012) and presumably contained record-setting amounts of SO_2 (http://en.wikipedia.org/wiki/2011_Nabro_eruption). It first propagated northward where it was registered at Mediterranean EARLINET stations. Our first detection took place much later, on 19 July. As in the case of the Sarychev plume first a spiky structure with pronounced intra-day variability was observed (water-vapour DIAL). In the second half of August, the aerosol settled into a broad hump peaking between 15 and 17 km.

5 Discussion and conclusions

The long background period after the end of the Pinatubo phase and recent moderate eruptions yield some insight into the processes maintaining the stratospheric aerosol layer. Tropospheric air pollution of both natural and anthropogenic origin can yield a minor contribution. Upward injection of tropospheric air into the stratosphere is most commonly achieved via deep convection or, at a level of several per cent, in the outflow of warm conveyor belts (WCBs; Stohl, 2001; Wernli and Bourqui, 2002; Sprenger and Wernli, 2003). Deep pyro-convection has been identified to yield occasional contribution slightly exceeding the 1997–2006 background (Sect. 3.3), the WCB mechanism seems to be more important for trace gases (Stohl and Trickl, 1999; Trickl et al., 2003) than for aerosols due to washout. Another possibility could be cross-tropopause transport following volcanic eruptions occurring directly in favourable regions in the vicinity of the jet stream, at least for small contributions to the lower-stratospheric aerosol budget.

The positive trend in stratospheric aerosol load observed over Mauna Loa and Boulder (Hofmann et al., 2009) starting as early as in 1998 is not visible in our data for such a long period of time and rather uncertain since the period with the lowest backscatter coefficients ended too early in autumn 2006. After major volcanic eruptions at low latitudes the maximum at our mid-latitude site occurs typically within half a year after the beginning of the eruption. Thus, one would expect an increase rather early. At least the next volcanic period, starting towards the end of 2006, makes any meaningful trend

ACPD
12, 23135–23193, 2012

determination impossible. The interpretation of their trends by Hofmann et al. (2009) by an impact of the growing Asian air pollution is, therefore, questionable. The influence of such a big source with continuous emissions should have led to a comparable increase in particles over Central Europe.

Vernier et al. (2011a) report on an aerosol layer in the subtropical tropopause region between the East Atlantic and the West Pacific, detected in CALIPSO measurements between 2006 and 2009. This is a region where strong vertical exchange in the vicinity of the subtropical jet stream can be expected (e.g., Sprenger et al., 2003; Trickl et al., 2011) and where also aerosols from minor volcanic eruptions could reach the stratosphere. Also upward transport of mineral dust is considered by Vernier et al. (2011a), but the data were selected for depolarization ratios for 5 % and less. The scattering ratio within this layer exhibits a pronounced seasonal cycle and a positive trend. Vernier et al. (2011b), by analysing satellite data, meanwhile ascribed the increase to volcanic eruptions in the (sub)tropics and rejected the coal-burning hypothesis. This is strongly supported by the results of our analysis (Sect. 3.2). There is a clear rise in volcanic activity in the tropics, much earlier than that in the mid-latitudes. Most importantly, there have been one and more eruptions per year reaching altitudes around the tropical tropopause.

After the El Chichon and Pinatubo eruptions the aerosol peak above Garmisch-Partenkirchen occurred roughly half a year later. The transfer from the tropics to the mid-latitudes was rather steady and could be resolved because of the high particle concentrations. In the case of the Soufrière Hills plume the peak was observed with a similar delay, but the observation was limited to a few days in December 2006. This suggests that the transfer between the two latitudes is episodic and related to favourable meteorological patterns. As a consequence, not all eruption plumes that are observed above Mauna Loa will yield a comparable signature above our site. One would expect a higher importance of the mid-latitude eruptions such as those on the Kuril Islands, in Kamchatka and in Alaska. This view is hardened by the difference in trend in Fig. 3.

ACPD
12, 23135–23193, 2012

Even during the background period contributions from minor eruptions cannot be excluded. For the mid-latitude volcanoes the tropopause is lower and eruptions can reach the tropopause region much easier. However, these contributions are difficult to resolve unless a plume passes our site on its first round trip on the Northern Hemisphere. Our trend analysis is limited to two years and, thus, insufficient for deriving a clear message. In any case, Martinsson et al. (2005) found a pronounced increase of sulphur-containing particles above the tropopause for CARIBIC (Civil Aircraft for Regular Investigation of the Atmosphere on an Instrument Container) flights during the period 1999–2002, i.e., when the stratospheric background was the lowest. This points to the presence of particles from volcanic eruptions.

In this context the Eyjafjallajökull eruption was ideal for estimating an impact of a minor event on the lower stratosphere because of its proximity. We could verify pronounced contributions around 3 km on all four days, 18, 19, 20 and 23 April. Our analysis yields advection of volcanic aerosol in the lower stratosphere on the first two measurement days, possibly also on the third, but in this case mixed with Asian dust. The reported maximum eruption altitudes between 8 and 9.3 km were, indeed, close to and sometimes above the tropopause level. Rising farther would require dynamical lifting or absorption of solar radiation by the particles (De Laat et al., 2012). The backscatter coefficients within the first 2 km above the tropopause exceed the stratospheric background by a factor of three to four.

Several minor eruption reaching altitudes around 10 km occurred in Kamchatka and on the Kuril Islands in late 2009 and early 2010. However, their impact could not be verified. The forward trajectories calculated for these eruptions do not reveal direct transport to Europe, the air masses obviously staying in regions around the volcanic sources for an extended period of time. Thus, significant vertically confined aerosol structures are less likely to have survived if Europe was eventually reached.

Acknowledgements. The authors thank the late R. Reiter, W. Seiler and H. P. Schmid for their support along this long measurements series. They remind of the important role of W. Carnuth for the lidar work at IFU, who built and applied the first version of the big aerosol and other

ACPD
12, 23135–23193, 2012

lidar systems. P. Keckhut provided temperature calculations with the MIMOSA model for the December-2006 episode, and M. Sprenger the daily forecast of stratospheric air intrusions. N. Kristiansen and S. Eckhardt made available the FLEXPART model run. This work was funded by the German Federal Ministry of Education and Research within the German Lidar Network and the European Union within the European Aerosol Research Lidar Network (EARLINET) and EARLINET-ASOS, and has contributed to the Network of Atmospheric Composition Change (NDACC).

The service charges for this open access publication have been covered by a Research Centre of the Helmholtz Association.

References

Ansmann, A., Tesche, M., Groß, S., Freudenthaler, V., Seifert, P., Hiebsch, A., Schmidt, J., Mattis, I., Wandinger, U., Müller, D., and Wiegner, M.: The 16 April 2010 major volcanic ash plume over Central Europe: EARLINET lidar and AERONET photometer observations at Leipzig and Munich, Germany, Geophys. Res. Lett., 37, L13810, doi:10.1029/2010GL043809, 2010.

Ansmann, A., Tesche, M., Seifert, P., Groß, S., Freudenthaler, V., Apituley, A., Wilson, K. M., Serikov, I., Linné, H., Heinold, B., Hiebsch, A., Schnell, F., Schmidt, J., Mattis, I., Wandinger, U., and Wiegner, M.: Ash and fine-mode particle mass profiles from EARLINET-AERONET observations over Central Europe after the eruptions of the Eyjafjallajökull volcano in 2010, J. Geophys. Res., 116, D00U02, doi:10.1029/2010JD015567, 2011.

Arason, P., Petersen, G. N., and Bjornsson, H.: Observations of the altitude of the volcanic plume during the eruption of Eyjafjallajökull, April–May 2010, Earth Syst. Sci. Data, 3, 9–17, doi:10.5194/essd-3-9-2011, 2011.

Bates, D. R.: Rayleigh scattering by air, Planet. Space. Sci., 32, 785–790, 1984.

Berresheim, H. and Jaeschke, W.: The contribution of volcanoes to the global atmospheric sulfur budget, J. Geophys. Res., 88, 3732–3740, 1983.

Bigg, E. K.: The detection of atmospheric dust and temperature inversions by twilight scattering, J. Meteorol., 13, 262–268, 1956.

ACPD

12, 23135–23193, 2012

Bingemer, H., Klein, H., Ebert, M., Haunold, W., Bundke, U., Herrmann, T., Kandler, K., Müller-Ebert, D., Weinbruch, S., Judt, A., Wéber, A., Nillius, B., Ardon-Dryer, K., Levin, Z., and Curtius, J.: Atmospheric ice nuclei in the Eyjafjallajökull volcanic ash plume, Atmos. Chem. Phys., 12, 857–867, doi:10.5194/acp-12-857-2012, 2012.

Bösenberg, J., Alpers, M., Althausen, D., Ansmann, A., Böckmann, C., Eixmann, R., Franke, A., Freudenthaler, V., Giehl, H., Jäger, H., Kreipl, S., Linné, H., Matthias, V., Mattis, I., Müller, D., Sarközi, J., Schneidenbach, L., Schneider, J., Trickl, T., Vorobieva, E., Wandinger, U., and Wiegner, M.: The German Aerosol Lidar Network: Methodology, Data, Analysis, Report Nr. 317, ISSN 0937–1060, Max-Planck-Institut für Meteorologie, Hamburg, Germany, 155 pp., 2001.

Bösenberg, J., Matthias, V., Amodeo, A., Amoiridis, V., Ansmann, A., Baldasano, J. M., Balin, I., Balis, D., Böckmann, C., Boselli, A., Carlsson, G., Chaikovski, A., Chourdakis, G., Comerón, A., De Tomasi, F., Eixmann, R., Freudenthaler, V., Giehl, H., Grigorov, I., Hågård, A., Iarlore, M., Kirsche, A., Kolarov, G., Komguem, L., Kreipl, S., Kumpf, W., Larchevêque, G., Linné, H., Matthey, R., Mattis, I., Mekler, A., Mironova, I., Mitev, V., Mona, L., Müller, D., Music. S., Nickovic, S., Pandolfi, M., Papayannis, A., Pappalardo, G., Pelon, J., Pérez, C., Perrone, R. M., Persson, R., Resendes, D. P., Rizi, V., Rocadenbosch, F., Rodrigues, J. A., Sauvage, L., Schneidenbach, L., Schumacher, R., Sherbakov, V., Simeonov, V., Sobolewski, P., Spinelli, N., Stachlewska, I., Stoyanov, D., Trickl, T., Tsaknakis, G., Vaughan, G., Wandinger, U., Wang, X., Wiegner, M., Zavrtanik, M., and Zerefos, C.: EARLINET: A European Aerosol Research Lidar Network to Establish an Aerosol Climatology, Report Nr. 348, ISSN 0937 1060, edited by: Bösenberg, J., Co-ordinator, Max-Planck-Institut für Meteorologie, Hamburg, Germany, 155 pp., 2003.

Bourassa, A. E., Degenstein, D. A., Elash, B. J., and Llewellyn, E. J.: Evolution of the stratospheric aerosol enhancement following the eruptions of Okmok and Kasatochi: Odin-OSIRIS measurements, J. Geophys. Res., 115, D00L03, doi:10.1029/2009JD013274, 2010.

Brion, J., Chakir, A., Charbonnier, J., Daumont, D., Parisse, C., and Malicet, J.: Absorption spectra measurements for the ozone molecule in the 350–830 nm region, J. Atmos. Chem., 30, 291–299, 1998.

Campbell, J. R., Welton, E. J., Krotkov, N. A., Yang, K., Stewart, S. A., and Fromm, M. D.: Liekely seeing of cirrus clouds by stratospheric Kasatochi volcanic aerosol particles near a mid-latitude tropopause fold, Atmos. Environ., 446, 441–448, 2012.

ACPD
12, 23135–23193, 2012

Charlson, R. J., Langner, J., Rodhe, H., Leovy C. B., and S. G. Warren: Perturbation of the Northern Hemisphere radiative balance by backscattering from anthropogenic sulfate aerosols, Tellus B, 43, 152–163, 1991.
Carnuth, W. and Trickl, T.: Transport studies with the IFU three-wavelength aerosol lidar during the VOTALP Mesolcina experiment, Atmos. Environ., 34, 1425–1434, 2000.
Carnuth, W., Kempfer, U., and Trickl, T.: Highlights of the tropospheric lidar studies at IFU within the TOR project, Tellus B, 54, 163–185, 2002.
Dacre, H. F., Grant, A. L. M., Hogan, R. J., Belcher, S. E., Thomson, D. J., Devenish, B, J., Marenco, F., Hort, M. C., Haywood, J. M., Ansmann, A., Mattis, I., and Clarisse, L.: Evaluating the structure and magnitude of the ash plume during the initial phase of the 2010 Eyjafjallajökull eruption using lidar observations and NAME simulations, J. Geophys. Res., 116, D00U03, doi:10.1029/2011JD015608, 2011.
De Laat, A. T. J., Stein Zweers, D. C., Boers, R., and Tuinder, O. N. E.: A solar escalator: observational evidence of the self-lifting of smoke and aerosols by absorption of solar radiation in the February 2009 Australian Black Saturday plume, J. Geophys. Res., D04204, doi:10.1029/2011JD017016, 2012.
Deshler, T.: A review of global stratospheric aerosol: measurements, importance, life cycle, and stratospheric aerosol, Atmos. Res., 90, 223–232, 2008.
Deshler, T., Anderson-Sprecher, R., Jäger, H., Barnes, J., Hofmann, D. J., Clemensha, B., Simonich, D., Grainger, R. G., and Godin-Beekmann, S.: Trends in the non-volcanic component of stratospheric aerosol over the period 1971–2004, J. Geophys. Res., 111, D01201, doi:10.1029/2005JD006089, 2006.
Draxler, R. and Hess, G.: An overview of the HYSPLIT_4 modelling system for trajectories, dispersion, and deposition, Aust. Meteorol. Mag., 47, 295–308, 1998.
Eisele, H., Scheel, H. E., Sladkovic, R., and Trickl, T.: High-resolution lidar measurements of stratosphere-troposphere exchange, J. Atmos. Sci., 56, 319–330, 1999.
Emeis, S., Forkel, R., Junkermann, W., Schäfer, K., Flentje, H., Gilge, S., Fricke, W., Wiegner, M., Freudenthaler, V., Groß, S., Ries, L., Meinhardt, F., Birmili, W., Münkel, C., Obleitner, F., and Suppan, P.: Measurement and simulation of the 16/17 April 2010 Eyjafjallajökull volcanic ash layer dispersion in the northern Alpine region, Atmos. Chem. Phys., 11, 2689–2701, doi:10.5194/acp-11-2689-2011, 2011.
Fernald, F. G.: Analysis of atmospheric lidar observations: some comments, Appl. Optics, 23, 652–653, 1984.

ACPD
12, 23135–23193, 2012

Fiocco, G. and Grams, G: Observations of the aerosol layer at 20 km by optical radar, J. Atmos. Sci., 21, 323–324, 1964.
Flentje, H., Claude, H., Elste, T., Gilge, S., Köhler, U., Plass-Dülmer, C., Steinbrecht, W., Thomas, W., Werner, A., and Fricke, W.: The Eyjafjallajökull eruption in April 2010 – detection of volcanic plume using in-situ measurements, ozone sondes and lidar-ceilometer profiles, Atmos. Chem. Phys., 10, 10085–10092, doi:10.5194/acp-10-10085-2010, 2010.
Forster, C., Wandinger, U., Wotawa, G., James, P., Mattis, I., Althausen, D., Simmonds, P., O'Doherty, S., Jennings, S. G., Kleefeld, C., Schneider, J., Trickl, T., Kreipl, S., Jäger, H., and Stohl, A.: Transport of boreal forest fire emissions from Canada to Europe, J. Geophys. Res., 106, 22887–22906, 2001.
Freudenthaler V.: Lidarmessungen der räumlichen Ausbreitung sowie mikrophysikalischer und optischer Parameter von Flugzeugkondesstreifen, (in German), Dissertation, Universität Hohenheim, Germany (1999) und Schriftenreihe des Fraunhofer-Instituts für Atmosphärische Umweltforschung, vol. 63, Shaker Verlag GmbH, Aachen, 2000, ISBN 3-8265-6973-3, ISSN 1436-1094, 134 pp., 2000.
Freudenthaler V., Homburg, F., and Jäger, H.: Ground-based mobile scanning LIDAR for remote sensing of contrails, Ann. Geophys., 12, 956–961, 1994, http://www.ann-geophys.net/12/956/1994/.
Freudenthaler, V., Homburg, F., and Jäger, H.: Contrail observations by ground-based mobile scanning lidar: cross-sectional growth, Geophys. Res. Lett., 22, 3501–3504, 1995
Fromm, M. and Servranckx, R.: Transport of forest fire smoke, above the tropopause, supercell convection, Geophys. Res. Lett., 30, 1542, doi:10.1029/2002GL016820, 2003.
Fromm, M., Alfred, J., Hoppel, K., Hornstein, J., Bevilacqua, R., Shettle, E., Servranckx, R., Li, Z., and Stocks, B.: Observations of boreal forest fire smoke in the stratosphere by POAM III, SAGE II, and lidar in 1998, Geophys. Res. Lett., 27, 1407–1410, 2000.
Fromm, M., Torres, O., Diner, D., Lindsey, D., Vant Hull, B., Servranckx, R., Shettle, E. P., and Li, Z.: Stratospheric impact of the Chisholm pyrocumulonimbus eruption: 1. Earth-viewing satellite perspective, J. Geophys. Res., 113, D08202, doi:10.1029/2007JD009153, 2008a.
Fromm, M., Shettle, E. P., Fricke, K. H., Ritter, C., Trickl, T., Giehl, H., Gerding, M., Barnes, J., O'Neill, M., Massie, S. T., Blum, U., McDermid, I. S., Leblanc, T., and Deshler, T.: The stratospheric impact of the Chisholm pyrocumulonimbus eruption: 2. vertical profile perspective, J. Geophys. Res., 113, D08203, doi:10.1029/2007JD009147, 2008b.

ACPD
12, 23135–23193, 2012

Fromm, M., Lindsey, D. T., Servranckx, R., Yue, G., Trickl, T., Sica, R., Doucet, P., and Godin-Beekmann, S.: The untold story of pyrocumulonimbus, B. Am. Meterol. Soc., 91, 1193–1209, 2010.

Gasteiger, J., Groß, S., Freudenthaler, V., and Wiegner, M.: Volcanic ash from Iceland over Munich: mass concentration retrieved from ground-based remote sensing measurements, Atmos. Chem. Phys., 11, 2209–2223, doi:10.5194/acp-11-2209-2011, 2011.

Gilge, S. and Plass-Dülmer, C.: Stark erhöhte SO_2-Konzentrationen an der Zugspitze infolge des Eyjafjallajökull-Ausbruchs, GAW-Brief des DWD, 51, Deutscher Wetterdienst, Offenbach, 2 pp., available at: http://www.dwd.de/gaw, (September 2012), 2010.

Grams, G. and Fiocco, G.: Stratospheric aerosol layer during 1964 and 1965, J. Geophys. Res., 72, 3523–3542, 1967.

Groß, S., Freudenthaler, V., Wiegner, M., Gasteiger, J., Geiß, A., and Schnell, F.: Dual-wavelength depolarization ratio of volcanic aerosols: lidar measurements of the Eyjafjallajökull plume over Maisach, Germany, Atmos. Environ., 48, 85–96, 2012.

Hansen, J., Sato, M., Lacis, A., and Ruedy, R.: The missing climate forcing, Philos. T. Roy. Soc. B, 352, 231–240, 1997.

Heue, K.-P., Brenninkmeijer, C. A. M., Wagner, T., Mies, K., Dix, B., Frieß, U., Martinsson, B. G., Slemr, F., and van Velthoven, P. F. J.: Observations of the 2008 Kasatochi volcanic SO_2 plume by CARIBIC aircraft DOAS and the GOME-2 satellite, Atmos. Chem. Phys., 10, 4699–4713, doi:10.5194/acp-10-4699-2010, 2010.

Hofmann, D., Barnes, J., O'Neill, M., Trudeau, M., and Neely, R.: Increase in background stratospheric aerosol observed with lidar at Mauna Loa Observatory and Boulder, Colorado, Geophys. Res. Lett., 36, L15808, doi:10.1029/2009GL039008, 2009.

Hoyle, C. R., Pinti, V., Welti, A., Zobrist, B., Marcolli, C., Luo, B., Höskuldsson, Á., Mattsson, H. B., Stetzer, O., Thorsteinsson, T., Larsen, G., and Peter, T.: Ice nucleation properties of volcanic ash from Eyjafjallajökull, Atmos. Chem. Phys., 11, 9911–9926, doi:10.5194/acp-11-9911-2011, 2011.

Jäger, H.: Long-term record of lidar observations of the stratospheric aerosol layer at Garmisch-Partenkirchen, J. Geophys. Res., 110, D08106, doi:10.1029/2004JD005506, 2005.

Jäger, H. and Deshler, T.: Lidar backscatter to extinction, mass and area conversions for stratospheric aerosols on midlatitude balloonborne size distribution measurements, Geophys. Res. Lett., 29, 1929, doi:10.1029/2002GL015609, 2002.

ACPD
12, 23135–23193, 2012

Jäger, H. and Deshler, T.: Correction to "Lidar backscatter to extinction, mass and area conversions for stratospheric aerosols on midlatitude balloonborne size distribution measurements", Geophys. Res. Lett., 30, 1382, doi:10.1029/2003GL017189, 2003.
Jäger, H. and Wege, K.: Stratospheric ozone depletion at northern midlatitudes after major volcanic eruptions, J. Atmos. Chem., 10, 273–287, 1990.
Jäger, H., Carnuth, W., and Georgi, B.: Observations of Saharan dust at a North Alpine station, J. Aerosol Sci., 19, 1235–1238, 1988.
Jäger, H., James, P., Stohl, A., and Trickl, T.: Long-range transport of free-tropospheric aerosol: a nine-year climatology, in: Reviewed and Revised Papers Presented at the 23rd International Laser Radar Conference, Nara (Japan), 24 to 28 July 2006, edited by: Nagasawa, C., Sugimoto, N., ISBN 4-9902916-0-3, Tokyo Metropolitan University, Tokyo, Japan, 795–796, 2006.
Junge, C. E. and Manson, J. E.: Stratospheric aerosol studies, J. Geophys. Res., 66, 2163–2182, 1961.
Keckhut, P., David, Ch., Marchand, M., Bekki, S., Jumelet, J., Hauchecorne, A., and Höpfner, M.: Observation of Polar Stratospheric Clouds down to the Mediterranean coast, Atmos. Chem. Phys., 7, 5275–5281, doi:10.5194/acp-7-5275-2007, 2007.
Klett, J. D.: Lidar inversion with variable backscatter/extinction ratios, Appl. Optics, 24, 1638–1643, 1985.
Kravits, B., Robock, A., Bourasa, A., Deshler, T., Wu, D., Mattis, I., Finger, F., Hoffmann, A., Ritter, C., Bitar, L., Duck, T., and Barnes, J. E.: Simulation and observations of stratospheric aerosols from the 2009 Sarychev volcanic eruption, J. Geophys. Res., 116, D18211, doi:10.1029/2010JD015501, 2011.
Martinsson, B. G., Nguyen, H. N., Brenninkmeijer, C. A. M., Zahn, A., Heintzenberg J., Hermann, M., and van Velthoven, P. F. J.: Characteristics and origin of lowermost stratospheric aerosol at northern midlatitudes under volcanically quiescent conditions based on CARIBIC observations, J. Geophys. Res., 110, D12201, doi:10.1029/2004JD005644, 2005.
Martinsson, B. G., Brenninkmeijer, C. A. M., Carn, S. A., Hermann, M., Heue, K.-P., van Velthoven, P. F. J., and Zahn, A.: Influence of the 2008 Kasatochi volcanic eruption on sulfurous and carbonaceous aerosol constituents in the lower stratosphere, Geophys. Res. Lett., 36, L12813, doi:10.1029/2009GL038735, 2009.
Massie, S. T.: Summary of volcanic activity, AURA Cloud/Aerosol/SO_2 Working Group, available at: http://avdc.gsfc.nasa.gov/, release April 2012. The data have been mostly extracted

ACPD
12, 23135–23193, 2012

from Smithsonian/USGS Weekly Volcanic Activity Report, http://volcano.si.edu/reports/usgs/index.cfm September 2012.

Mattis, I., Ansmann, A., Müller, D., Wandinger, U., and Althausen, D.: Multiyear aerosol observations with dual-wavelength Raman lidar in the framework of EARLINET, J. Geophys. Res., 109, D13203, doi:10.1029/2004JD004600, 2004.

Mattis, I., Seifert, P., Müller, D., Tesche, M., Hiebsch, A., Kanitz, T., Schmidt, J., Finger, F., Wandinger, U., and Ansmann, A.: Volcanic aerosol layers observed with multiwavelength Raman lidar over Central Europe in 2008–2009, J. Geophys. Res., 115, D00L04, doi:10.1029/2009JD013472, 2010.

Mona, L., Amodeo, A., D'Amico, G., Giunta, A., Madonna, F., and Pappalardo, G.: Multiwavelength Raman lidar observations of the Eyjafjallajökull volcanic cloud over Potenza, Southern Italy, Atmos. Chem. Phys., 12, 2229–2244, doi:10.5194/acp-12-2229-2012, 2012.

Nakada, E.: Special issue: the 2000 eruption of Miyakejima volcano, Japan, B. Volcanol., 67, 203–204, 2005.

Owens, J. C.: Optical refractive index of air: dependence on pressure, temperature and composition, Appl. Optics, 6, 51–60, 1967.

Papayannis, A., Amiridis, V., Mona, L., Tsaknakis, G., Balis, D., Bösenberg, J., Chaikovski, A. De Tomasi, F., Grigorov, I., Mattis, I., Mitev, V., Müller, D., Nickovic, S., Pérez, C., Pietruczuk, A., Pisani, G., Ravetta, F., Rizi, V., Sicard, M., Trickl, T., Wiegner, M., Gerding, M., Mamouri, R. E., D'Amico, G., and Pappalardo, G.: Systematic lidar observations of Saharan dust over Europe in the frame of EARLINET (2000–2002), J. Geophys. Res., 113, D10204, doi:10.1029/2007JD009028, 2008.

Pappalardo, G., Mona, L., D'Amico, G., Adam, M., Amodeo, A., Ansmann, A., Apituley, A., Alados Arboledas, L., Chaikovsky, A., Cuesta, J., De Tomasi, F., Freudenthaler, V., Giannakaki, E., Giehl, H., Giunta, A., Grigorov, I., Gross, S., Haeffelin, M., Iarlori, M., Linné, H., Madonna, F., Rodanthi Mamouri, E., Molero, F., Müller, D., Mitev, V. Nicolae, D., Pietruczuk, A., Pisani, G., Pujadas, M., Serikov, I., Sicard, M., Simeonov, V., Spinelli, N., Stebel, K., Trickl, T., Wandinger, U., Wagner, F., and Wiegner, M.: 4-D distribution of the 2010 Eyjafjallajökull volcanic cloud over Europe observed by EARLINET, in preparation for this special section, 2012.

Petersen, G. N.: A short meteorological overview of the Eyjafjallajökull eruption 14 April–23 May 2010, Weather, 65, 203–207, 2010.

ACPD
12, 23135–23193, 2012

Pittock, A. B.: Possible destruction of ozone by volcanic material at 50 mbar, Nature, 207, 182, 1965.
Prata, A. J., Carn, S. A., Stohl, A., and Kerkmann, J.: Long range transport and fate of a stratospheric volcanic cloud from Soufrière Hills volcano, Montserrat, Atmos. Chem. Phys., 7, 5093–5103, doi:10.5194/acp-7-5093-2007, 2007.
Rauthe-Schöch, A., Weigelt, A., Hermann, M., Martinsson, B. G., Baker, A. K., Heue, K.-P., Brenninkmeijer, C. A. M., Zahn, A., Scharffe, D., Eckhardt, S., Stohl, A., and van Velthoven, P. F. J.: CARIBIC aircraft measurements of Eyjafjallajökull volcanic clouds in April/May 2010, Atmos. Chem. Phys., 12, 879–902, doi:10.5194/acp-12-879-2012, 2012.
Reiter, R. and Carnuth, W.: Comparing lidar reflectivity profiles against measured profiles of vertical aerosol distribution between 1 and 3 km a.s.l., Arch. Meteor. Geophy. A, 24, 69–92, 1975.
Reiter, R., Jäger, H., Carnuth, W., and Funk, W.: The stratospheric aerosol layer observed by lidar since October 1976. A contribution to the problem of hemispheric climate, Arch. Meteor. Geophy. B, 27, 121–149, 1979.
Robock, A: Volcanic eruptions and climate, Rev. Geophys., 38, 191–219, 2000.
Robock, A. and Free, M. P.: Ice cores as an index of global volcanism from 1850 to the present, J. Geophys. Res., 100, 11549–11567, 1995.
Schumann, U., Weinzierl, B., Reitebuch, O., Schlager, H., Minikin, A., Forster, C., Baumann, R., Sailer, T., Graf, K., Mannstein, H., Voigt, C., Rahm, S., Simmet, R., Scheibe, M., Lichtenstern, M., Stock, P., Rüba, H., Schäuble, D., Tafferner, A., Rautenhaus, M., Gerz, T., Ziereis, H., Krautstrunk, M., Mallaun, C., Gayet, J.-F., Lieke, K., Kandler, K., Ebert, M., Weinbruch, S., Stohl, A., Gasteiger, J., Groß, S., Freudenthaler, V., Wiegner, M., Ansmann, A., Tesche, M., Olafsson, H., and Sturm, K.: Airborne observations of the Eyjafjalla volcano ash cloud over Europe during air space closure in April and May 2010, Atmos. Chem. Phys., 11, 2245–2279, doi:10.5194/acp-11-2245-2011, 2011.
Seifert, P., Ansmann, A., Groß, S., Freudenthaler, V., Heinold, B., Hiebsch, A., Mattis, I., Schmidt, J., Schnell, F., Tesche, M., Wandinger, U., and Wiegner, M.: Ice formation in ash-influenced clouds after the eruption, of the Eyjafjallajökull volcano in April 2010, J. Geophys. Res., 116, D00U04, doi:10.1029/2011JD015702, 2011.
Solomon, S.: Stratospheric ozone depletion: a review of concepts and history, Rev. Geophys., 37, 275–316, 1999.

ACPD
12, 23135–23193, 2012

Solomon, S., Portmann, R. W., Garcia, R., Thomason, L. W., Poole, L. R., and McCormick, M. P.: The role of aerosol variations in anthropogenic ozone depletion at northern midlatitudes, J. Geophys. Res., 101, 6713–6727, 1996.

Solomon, S., Daniel, J. S., Neely III, R. R., Vernier, J.-P., Dutton, E. G., and Thomason, L. W.: The persistently variable "background" stratospheric aerosol layer and global climate change, Science, 333, 866–870, 2011.

Sprenger, M. and Wernli, H.: A northern hemispheric climatology of cross-tropopause exchange for the ERA15 time period (1979–1993), J. Geophys. Res., 108, 8521, doi:10.1029/2002JD002636, 2003.

Sprenger, M., Croci Maspoli, M., and Wernli, H.: Tropopause folds and cross-tropopause exchange: a global investigation based upon ECMWF analyses for the time period March 2000 to February 2001, J. Geophys. Res., 108, 8518, doi:10.1029/2002JD002587, 2003.

Steinke, I., Möhler, O., Kiselev, A., Niemand, M., Saathoff, H., Schnaiter, M., Skrotzki, J., Hoose, C., and Leisner, T.: Ice nucleation properties of fine ash particles from the Eyjafjallajökull eruption in April 2010, Atmos. Chem. Phys., 11, 12945–12958, doi:10.5194/acp-11-12945-2011, 2011.

Stohl, A.: A 1-year Lagrangian "climatology" of airstreams in the Northern Hemisphere troposphere and lowermost stratosphere, J. Geophys. Res., 106, 7263–7279, 2001.

Stohl, A. and Trickl, T.: A textbook example of long-range transport: simultaneous observation of ozone maxima of stratospheric and North American origin in the free troposphere over Europe, J. Geophys. Res., 104, 30445–30462, 1999.

Tesche, M., Glantz, P., Johansson, C., Norman, M., Hiebsch, A., Ansmann, A., Althausen, D., Engelmann, R., and Seifert, P.: Volcanic ash over Scandinavia originating from the Grímsvötn eruptions in May 2011, J. Geophys. Res., 117, D09201, doi:10.1029/2011JD017090, 2012.

Trickl, T.: Upgraded 1.56-µm lidar at IMK-IFU with 0.28 J/pulse, Appl. Optics, 49, 3732–3740, 2010.

Trickl, T. and Wanner, J.: The dynamics of the reactions F + IX → IF + X (X = Cl, Br, I); a laser-induced fluorescence study, J. Chem. Phys., 78, 6091–6101, 1983.

Trickl, T and Wanner, J.: High-resolution, laser-induced fluorescence spectroscopy of nascent IF: determination of X- and B-state molecular constants, J. Mol. Spectrosc., 104, 174–182, 1984.

ACPD
12, 23135–23193, 2012

Trickl, T., Cooper, O. C., Eisele, H., James, P., Mücke, R., and Stohl, A.: Intercontinental transport and its influence on the ozone concentrations over Central Europe: three case studies, J. Geophys. Res., 108, 8530, doi:10.1029/2002JD002735, 2003.

Trickl, T., Feldmann, H., Kanter, H.-J., Scheel, H.-E., Sprenger, M., Stohl, A., and Wernli, H.: Forecasted deep stratospheric intrusions over Central Europe: case studies and climatologies, Atmos. Chem. Phys., 10, 499–524, doi:10.5194/acp-10-499-2010, 2010.

Trickl, T., Bärtsch-Ritter, N., Eisele, H., Furger, M., Mücke, R., Sprenger, M., and Stohl, A.: High-ozone layers in the middle and upper troposphere above Central Europe: potential import from the stratosphere along the subtropical jet stream, Atmos. Chem. Phys., 11, 9343–9366, doi:10.5194/acp-11-9343-2011, 2011.

Vernier, J.-P., Thomason, and Kar, J.: CALIPSO detection of an Asian tropopause aerosol layer, Geophys. Res. Lett., 38, L07804, doi:10.1029/2010GL046614, 2011a.

Vernier, J.-P., Thomason, L. W., Pommereau, J.-P., Bourassa, A., Pelon, J., Garnier, A., Hauchecorne, A., Blanot, L., Trepte, C., Degenstein, D., and Vargas, F.: Major influence of tropical volcanic eruptions on the stratospheric aerosol layer during the last decade, Geophys. Res. Lett., 38, L12807, doi:10.1029/2011GL047563, 2011b.

Vogelmann, H. and Trickl, T.: Wide-range sounding of free-tropospheric water vapor with a differential-absorption lidar (DIAL) at a high-altitude station, Appl. Optics, 47, 2116–2132, 2008.

Vogelmann, H., Sussmann, R., Trickl, T., and Borsdorff, T.: Intercomparison of atmospheric water vapor soundings from the differential absorption lidar (DIAL) and the solar FTIR system on Mt. Zugspitze, Atmos. Meas. Tech., 4, 835–841, doi:10.5194/amt-4-835-2011, 2011.

Wernli, H. and Bourqui, M.: A Lagrangian "1-year climatology" of (deep) cross-tropopause exchange in the extratropical Northern Hemisphere, J. Geophys. Res., 107, 4021, doi:10.1029/2001JD000812, 2002.

Wirth, M., Fix, A., Ehret, G., Reichardt, J., Begie, R., Engelbart, D., Vömel, H., Calpini, B., Romanens, G., Apituley, A., Wilson, K. M., Vogelmann, H., and Trickl, T.: Intercomparison of airborne water vapour DIAL measurements with ground based remote sensing and radiosondes within the framework of LUAMI 2008, Contribution S07-P01-1 (3 pp.), in: Proceedings of the 8th International Symposium on Tropospheric Profiling (ISTP2009), Delft (The Netherlands), 19 to 23 October 2009, edited by: Apituley, A., Russchenberg, H. W. J., Monna, W. A. A., ISBN 978-90-6960-233-2, available at: http://cerberus.rivm.nl/ISTP/pages/index.htm (September 2012), RIVM, The Netherlands, 2009.

ACPD
12, 23135–23193, 2012

Zanis, P., Trickl, T., Stohl, A., Wernli, H., Cooper, O., Zerefos, C., Gaeggeler, H., Schnabel, C., Tobler, L., Kubik, P. W., Priller, A., Scheel, H. E., Kanter, H. J., Cristofanelli, P., Forster, C., James, P., Gerasopoulos, E., Delcloo, A., Papayannis, A., and Claude, H.: Forecast, observation and modelling of a deep stratospheric intrusion event over Europe, Atmos. Chem. Phys., 3, 763–777, doi:10.5194/acp-3-763-2003, 2003.

ACPD
12, 23135–23193, 2012

Table 1. List of volcanic eruptions between 40° N and 65° N reaching at least about 10 km (2004–2011); numbers in bold highlight top altitudes of 12 km and more. The information was extracted from Massie (2012), and between 2000 and April 2004 from http://www.volcano.si.edu, as well as other sources.

Date/Period	Volcano	Location	Maximum plume altitude [km]
18 Aug 2000	Miyake-Jima	Japan	**16**[a]
19 Feb 2001	Cleveland	Aleutian Islands	> 10
22 May 2001	Shiveluch	Kamtchatka	**20**
7 Jul 2001	Bezymianny	Kamtchatka	10
26 Jul 2003	Bezymianny	Kamtchatka	8–11
9–12 May 2004	Shiveluch	Kamtchatka	11
19 Jun 2004	Bezymianny	Kamtchatka	10
1 Nov 2004	Grimsvötn	Iceland	**12**
11 Jan 2005	Bezymianny	Kamtchatka	10
8 Mar 2005	St. Helens	Washington	11
6–7 Jul 2005	Shiveluch	Kamtchatka	10
11, 13 Jan 2006	Augustine	Alaska	10.4
27, 30 Jan 2006	Augustine	Alaska	**12.2**
9 May 2006	Bezymianny	Kamtchatka	**15**
24 Dec 2006	Bezymianny	Kamtchatka	10
16–28 Dec 2006	Shiveluch	Kamtchatka	10
1–26 Jan 2007	Shiveluch	Kamtchatka	**13.7**
29–30 Mar 2007	Shiveluch	Kamtchatka	**12.2**
9–11 Jun 2007	Kliuchevskoi	Kamtchatka	11
3–21 Aug 2007	Shiveluch	Kamtchatka	10
12 Jul 2008	Okmok	Aleutian Islands	**15**
17–30 Jul 2008	Okmok	Aleutian Islands	**12.2**
2–5 Aug 2008	Okmok	Aleutian Islands	10.7
7–9 Aug 2008	Kasatochi	Aleutian Islands	**13.7**
22–23 Mar 2009	Redoubt	Alaska	**19.8**
4–7 Apr 2009	Redoubt	Alaska	**15.2**
16 Jun 2009	Sarychev	Kuril Islands	9.7 (**12–18**[b])
15 Oct 2009	Ebeko	Kuril Islands	10.7
17 Dec 2009	Bezymianny	Kamtchatka	10
22–23 Jan 2010	Kliuchevskoi	Kamtchatka	10.1
14–15 Apr 2010	Eyjafjallajökull	Iceland	≥ 8 (until early 18 Apr[c])
1 Jun 2010	Bezymianny	Kamtchatka	10
1–11 Oct 2010	Kliuchevskoi	Kamtchatka	10.1
28 Oct–14 Nov 2010	Shiveluch	Kamtchatka	**12**
13 Dec 2010	Kizimen	Kamtchatka	10
23–25 Jan 2011	Kizimen	Kamtchatka	10
18 Apr 2011	Karymski	Kamtchatka	**11.9**
3–4 May 2011	Kizimen	Kamtchatka	10
21–24 May 2011	Grimsvötn	Iceland	**20**
27–31 May 2011	Shiveluch	Kamtchatka	10
3–21 Jun 2011	Shiveluch	Kamtchatka	10
9–15 Sep	Shiveluch	Kamtchatka	10.3
13–21 Oct	Shiveluch	Kamtchatka	10.6

[a] From Nakada (2005).

[b] From http://www.volcanodiscovery.com/sarychev.html; the eruption maximum is reported here for 15 June.

[c] Radar measurements show a maximum of 9.5 km (9.3 km) at the beginning and more than 8 km several times until early 18 April (Petersen, 2010; Arason et al., 2011).

ACPD
12, 23135–23193, 2012

Table 2. Tropopause altitude (TPA) and maximum relative humidity (MRH) between TPA – 3 km and TPA for Keflavik (Iceland) and Munich (Germany) for the relevant period in April 2010; in the presence of several temperature edges the one closest to the final drop in relative humidity was selected.

Day	Time [UTC]	TPA [km] Keflavik (Iceland)	MRH [%] Keflavik (Iceland)	TPA [km] Munich (Germany)	MRH [%] Munich (Germany)
13 Apr	00:00	11.1	47	8.0	52
	12:00	11.4	60	9.9	36
14 Apr	00:00	10.2	40	9.0	93
	12:00	8.9	38	9.7	69
15 Apr	00:00	9.4	76	8.1	89
	12:00	9.9	69	7.6	57
16 Apr	00:00	9.5	79	9.3	81
	12:00	7.4	37	9.7	30
17 Apr	00:00	6.9	23	9.8	36
	12:00	9.4	33	10.1	40
18 Apr	00:00	10.7	57	10.3	32
	12:00	9.9	85	9.6	63
19 Apr	00:00	9.7	54	n.a.	n.a.
	06:00	n.a.	n.a.	10.0	42
	12:00	9.5	55	10.3	47
	18:00	n.a.	n.a.	10.1	52
20 Apr	00:00	10.2	58	10.7	45
	06:00	n.a.	n.a.	10.3	39
	12:00	10.7	58	10.4	26
	18:00	n.a.	n.a.	10.1	59
21 Apr	00:00	10.1	57	10.1	66
	06:00	n.a.	n.a.	10.5	26
	12:00	10.6	29	10.7	22
	18:00	n.a.	n.a.	11.1	19
22 Apr	00:00	10.1	61	11.3	27
	06:00	n.a.	n.a.	11.1	56
	12:00	8.7	68	11.5	67
	18:00	n.a.	n.a.	10.7	35
23 Apr	00:00	8.9	17	11.3	44
	06:00	n.a.	n.a.	11.9	53
	12:00	9.6	41	11.8	69
	18:00	n.a.	n.a.	11.7	60
24 Apr	00:00	9.6	40	11.6	72

ACPD
12, 23135–23193, 2012

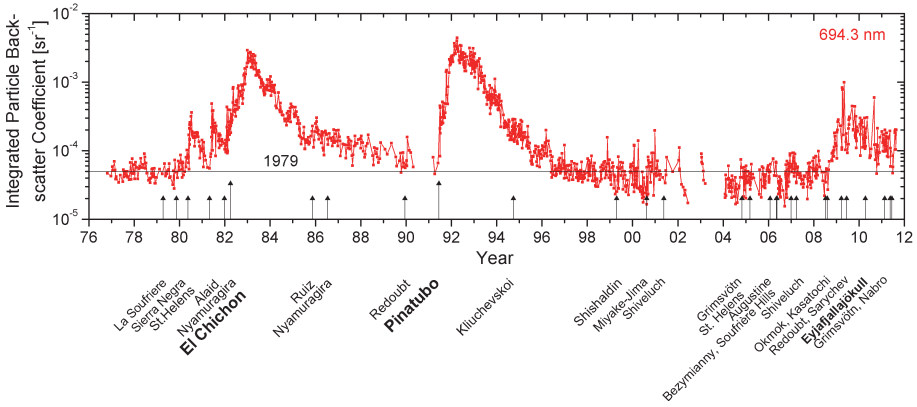

Fig. 1. Time series of the integrated stratospheric backscatter coefficient from the lidar measurements at Garmisch-Partenkirchen: the backscatter coefficients are integrated from 1 km above the tropopause to the upper end of the layer.

ACPD
12, 23135–23193, 2012

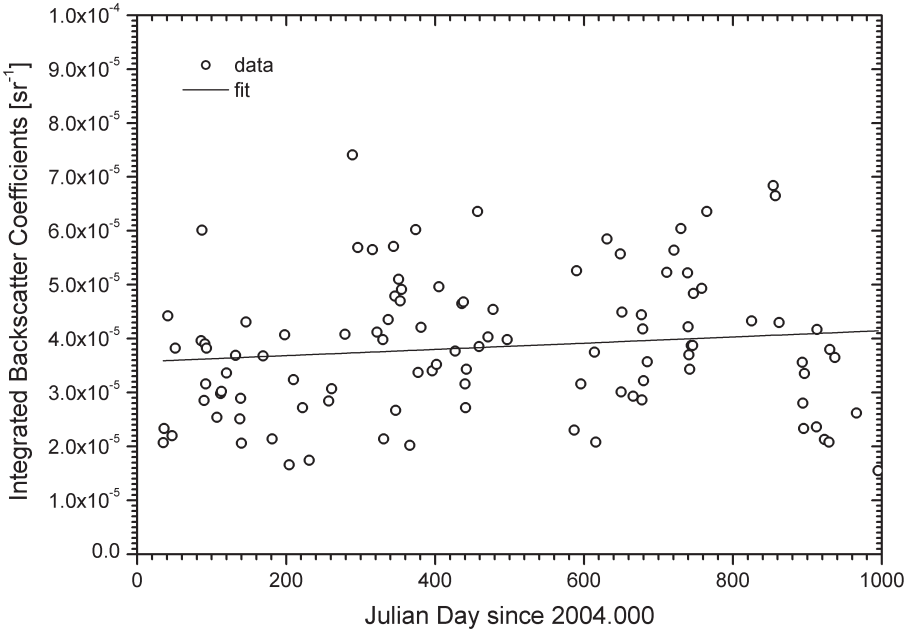

Fig. 2. Integrated backscatter coefficients from the NDACC lidar measurements between 2 February 2004 and 2 September 2006, and the result of a linear least-squares fit.

ACPD
12, 23135–23193, 2012

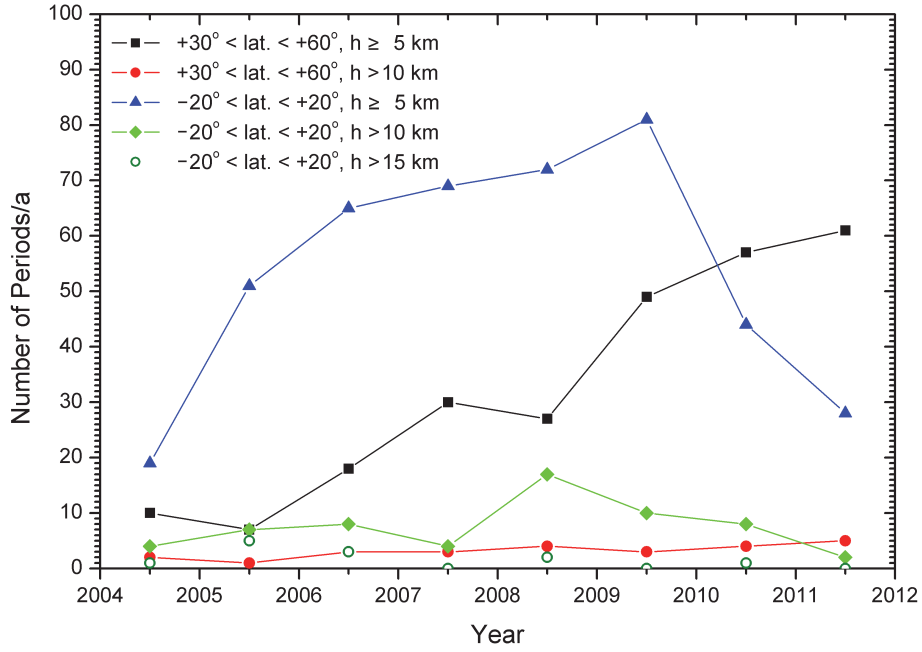

Fig. 3. Number of days our periods of uninterrupted volcanic activity per year derived from the listings by Massie (2012). There is a pronounced difference between the equatorial regions and higher latitudes of the Northern Hemisphere.

ACPD
12, 23135–23193, 2012

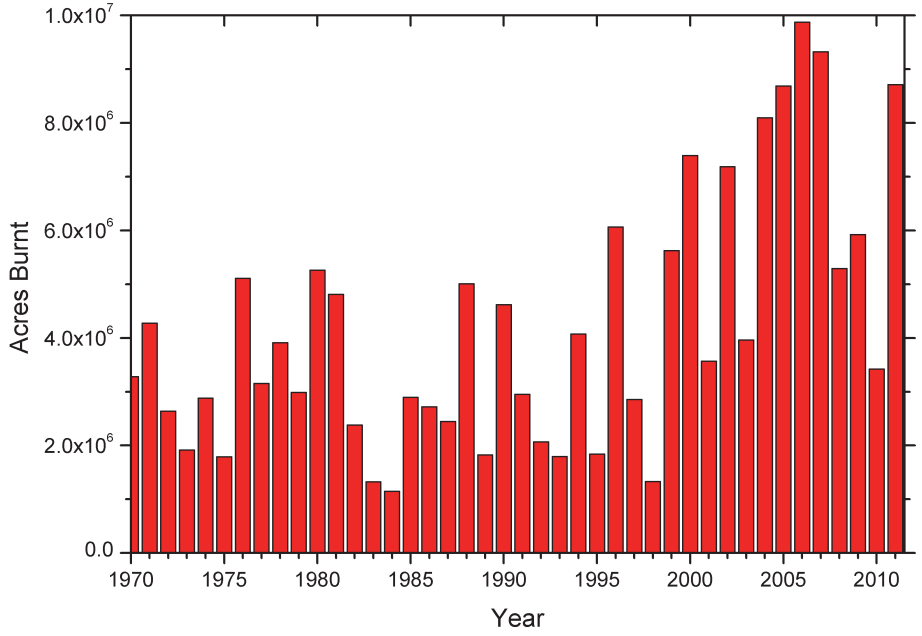

Fig. 4. Number of acres burnt per year in the United States of America (1960–2011); the numbers were taken from the National Interagency Fire Center (http://www.nifc.gov/).

ACPD
12, 23135–23193, 2012

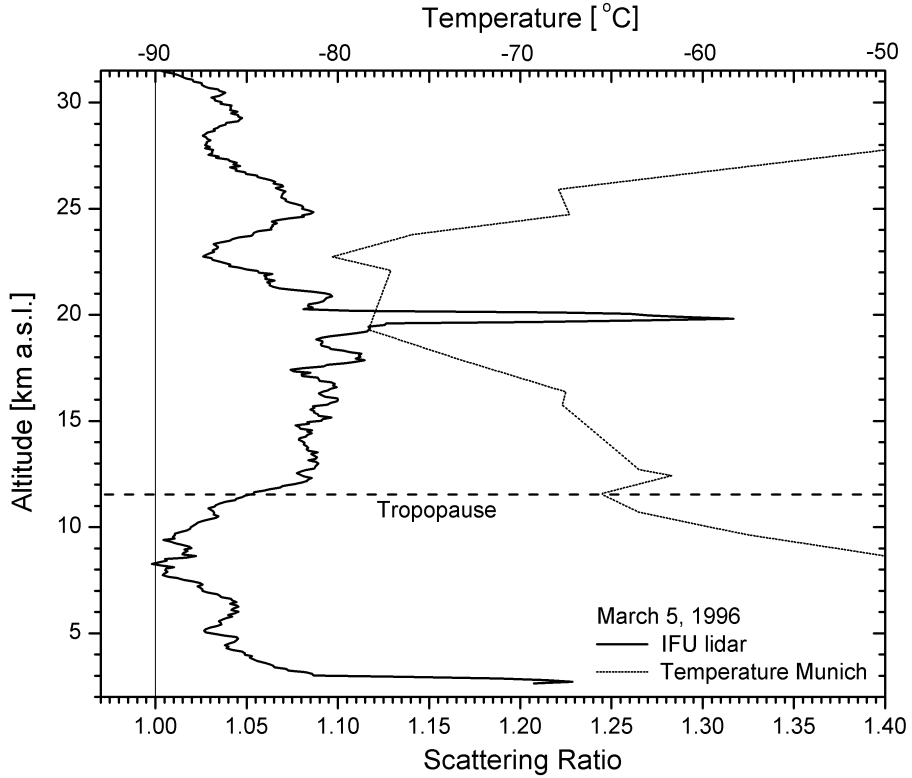

Fig. 5. Polar stratospheric cloud observed over Garmisch-Partenkirchen at about 20 km on 5 March 1996 (532 nm).

ACPD
12, 23135–23193, 2012

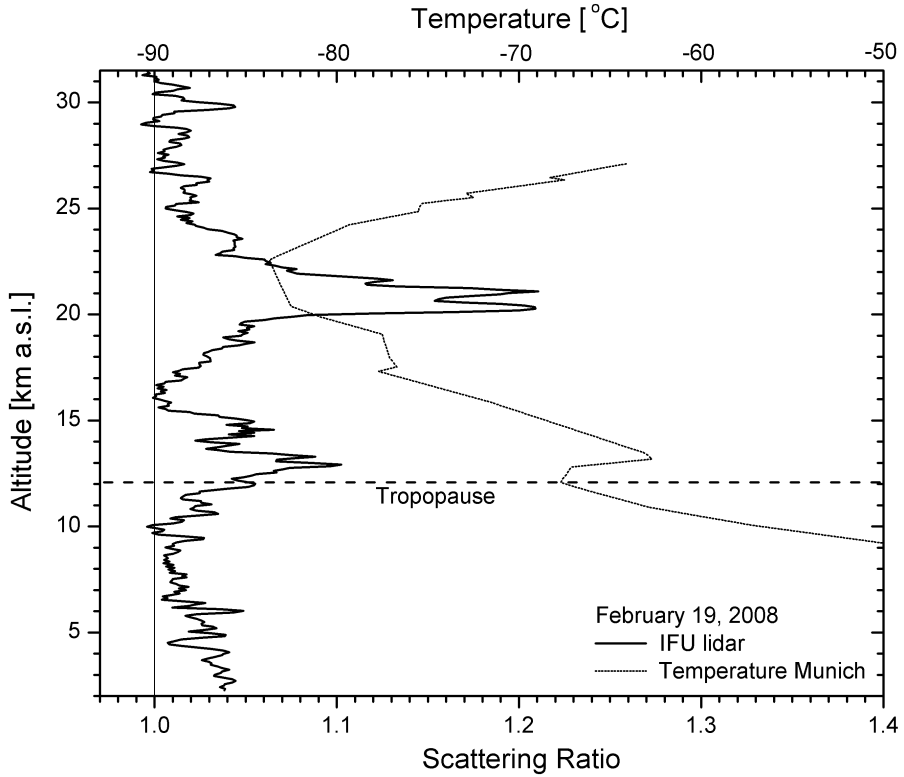

Fig. 6. Polar stratospheric cloud observed over Garmisch-Partenkirchen at about 21 km on 19 February 2008 (532 nm).

ACPD
12, 23135–23193, 2012

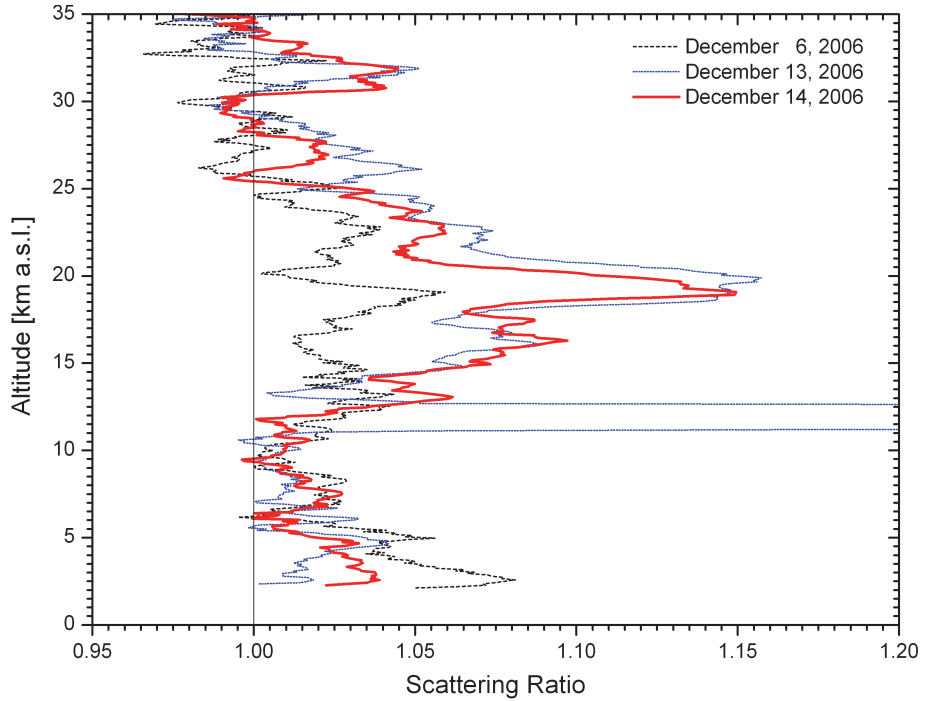

Fig. 7. 532-nm scattering ratios from December 2006 showing the sudden rise in stratospheric loading after a long background period characterized by values mostly below 1.05, i.e., 5 % above Rayleigh conditions.

ACPD
12, 23135–23193, 2012

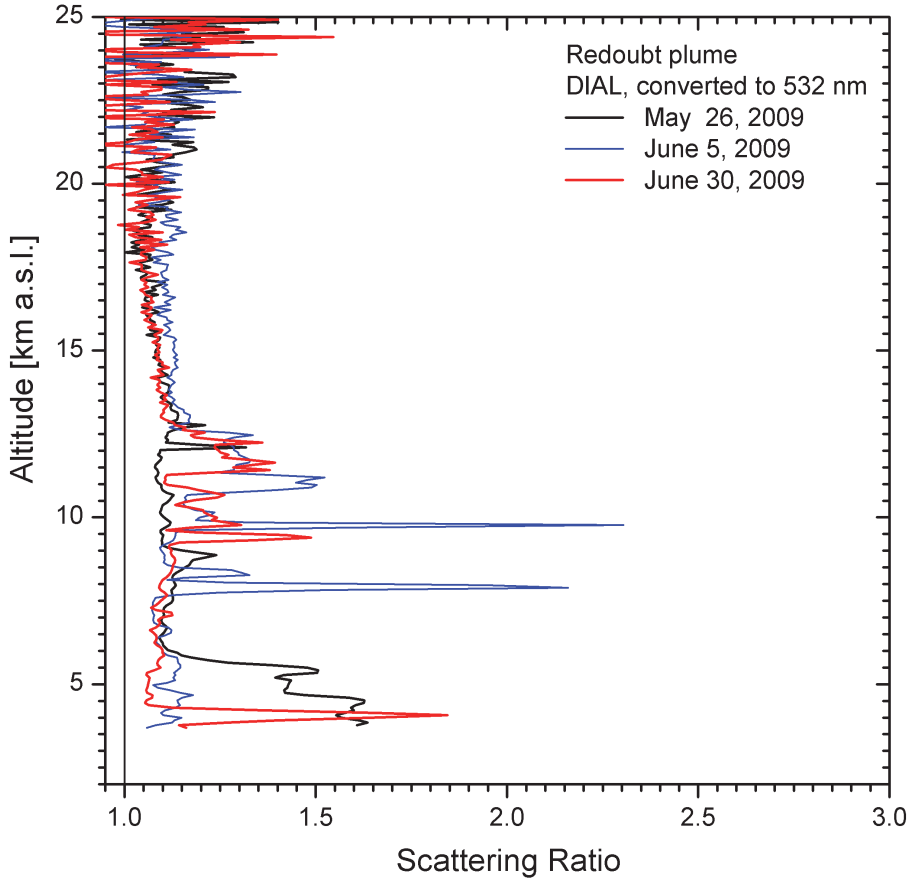

Fig. 8. Examples of 532-nm scattering ratios from the DIAL in May and June 2009, showing the signature of the Redoubt plume; the strong increase in noise and uncertainty above 15 km is due to the normalization to density (division by Rayleigh backscatter coefficients).

ACPD
12, 23135–23193, 2012

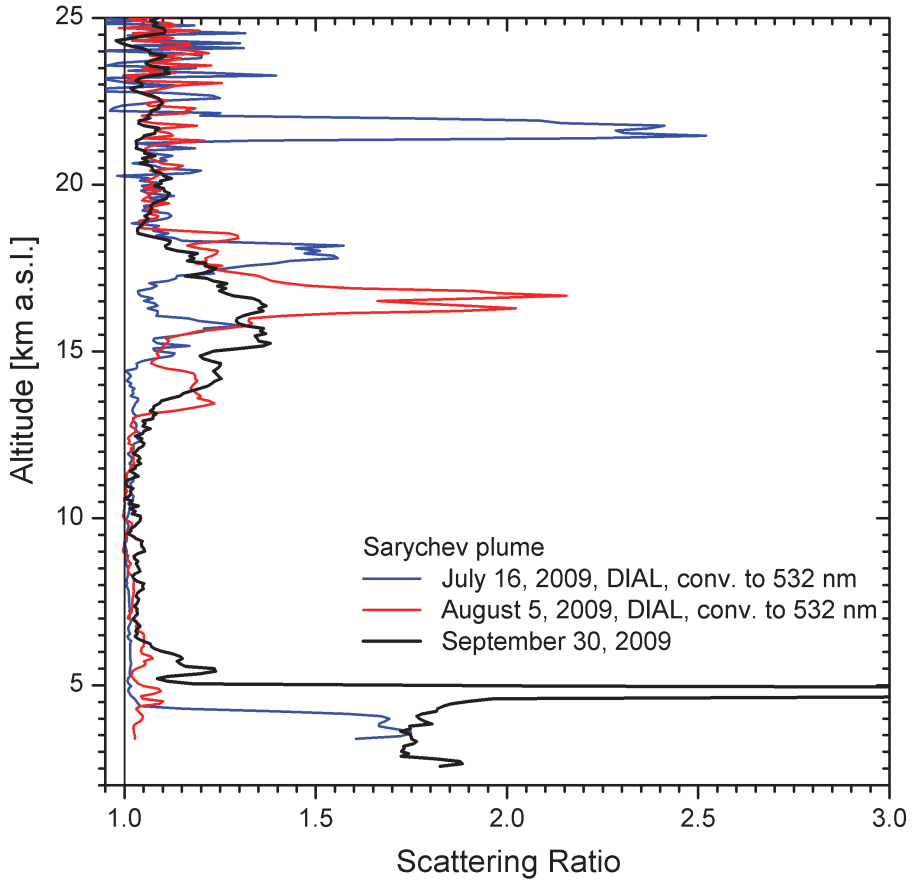

Fig. 9. Examples of 532-nm scattering ratios in from July to September, 2009, showing the signature of the Sarychev plume; the signal of the NDACC lidar was low in the third example due to pronounced light extinction in the aerosol layer below 5 km and is, therefore, averaged between 6.3 and 12 km to reduce the noise.

ACPD
12, 23135–23193, 2012

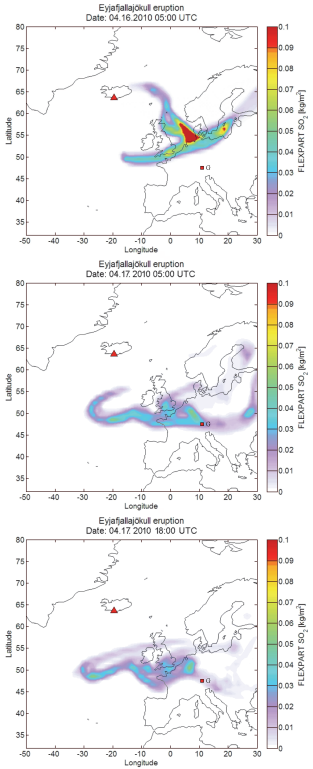

Fig. 10. Examples from calculations with the FLEXPART dispersion model on 21 April 2010 (source: N. Kristiansen and S. Eckhardt, NILU, Norway); the eruption period chosen in the simulation was 14 April 18:00 UTC, to 15 April 18:00 UTC. The images show SO_2 mass columns. The position of Eyjafjallajökull is marked by a red triangle, that of Garmisch-Partenkirchen by a red square.

ACPD
12, 23135–23193, 2012

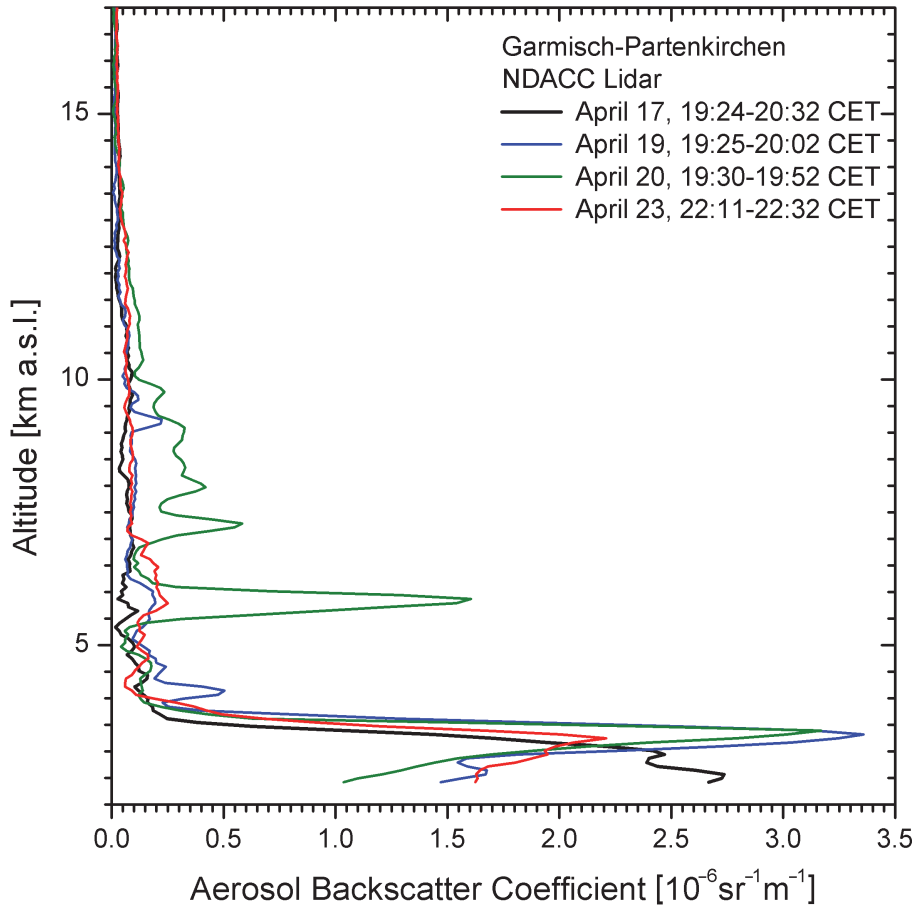

Fig. 11. The 532-nm aerosol backscatter coefficients from the NDACC lidar on all four relevant measurement evenings in April 2010. Three-point arithmetic averaging was applied for reducing the noise.

ACPD
12, 23135–23193, 2012

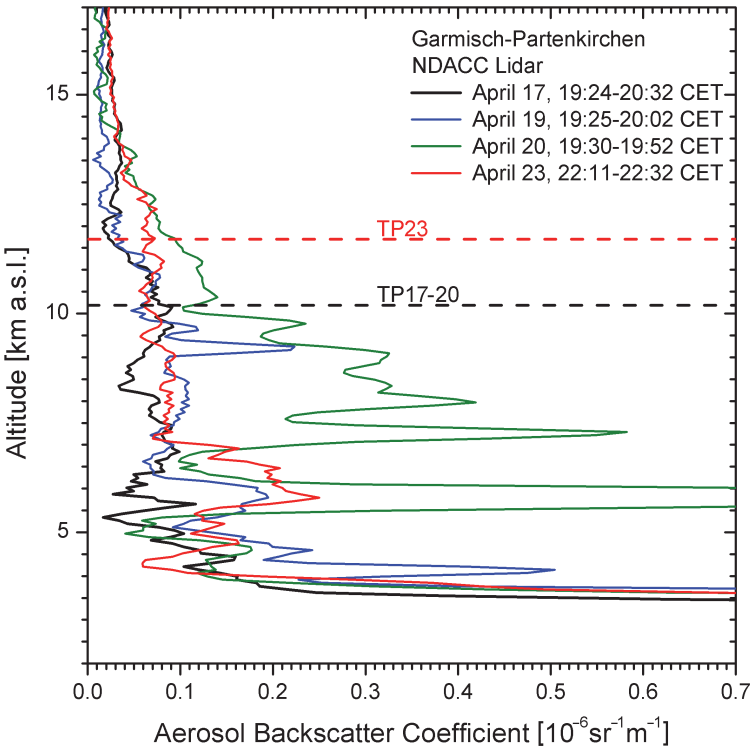

Fig. 12. Enlarged version of Fig. 11; the average Munich tropopause position for the period 17 to 20 April 2010 (TP17–23), and that of 23 April 2010, 19:00 CET (TP23) are given. The tropopause was 10.18 km ± 0.35 km from 17 April to the middle of 21 April (Column 3 of Table 2). It then grew to almost 12 km.

ACPD
12, 23135–23193, 2012

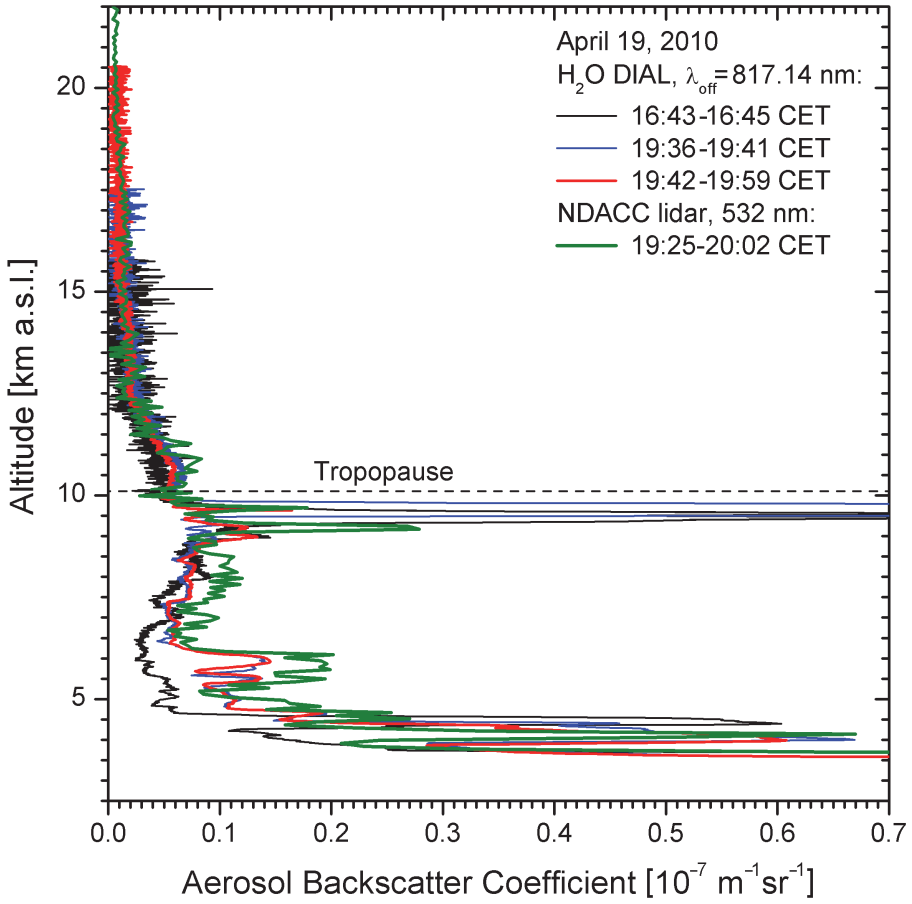

Fig. 13. The aerosol backscatter coefficients from the Zugspitze DIAL (817 nm) on 19 April 2010, together with the profile from the NDACC lidar (532 nm) for the same day.

ACPD
12, 23135–23193, 2012

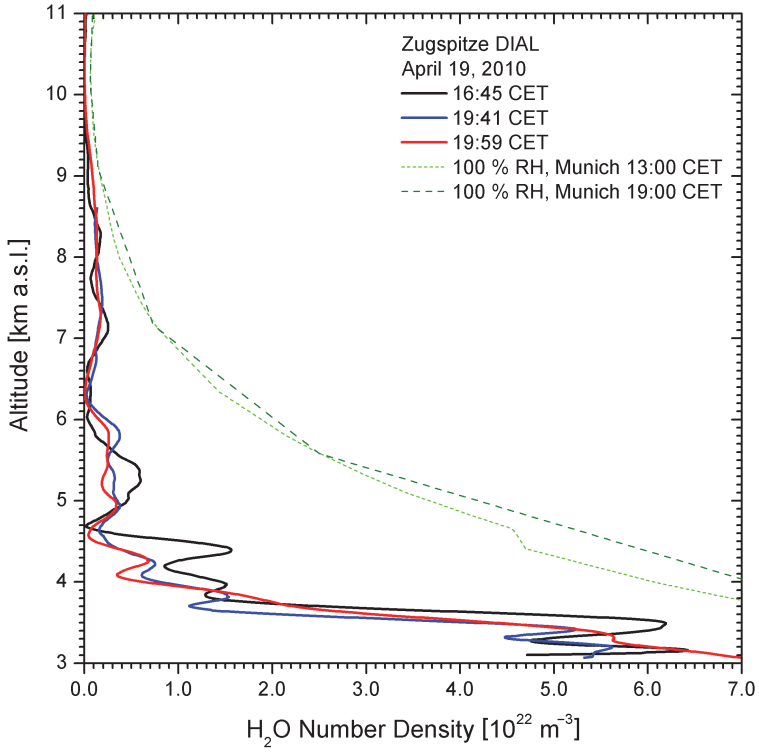

Fig. 14. Water-vapour profiles from the Zugspitze DIAL (817 nm) on 19 April 2010, obtained from the same measurements as those underlying Fig. 13. The times given are end times (see Fig. 13). The dashed curves give the H_2O densities calculated from two radiosonde ascents at Oberschleißheim ("Munich" sonde) 100 km roughly to the north of IMK-IFU. The uncertainty level for the lidar measurements above 8 km is estimated as less than 5×10^{-20} m^{-3}.

ACPD
12, 23135–23193, 2012

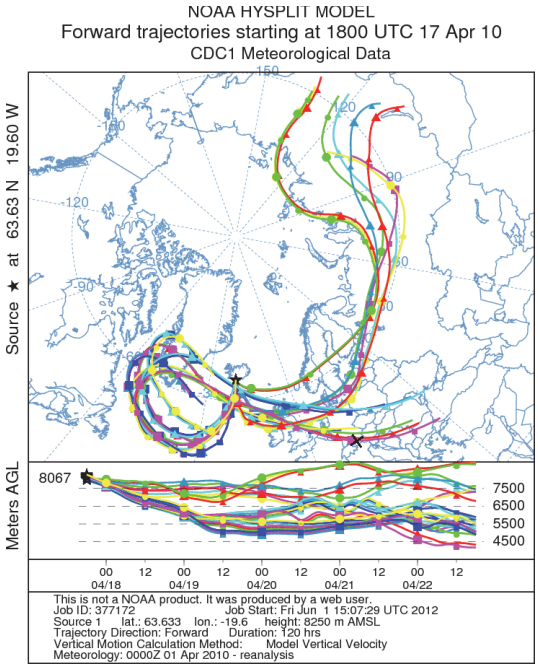

Fig. 15. HYSPLIT forward ensemble trajectories initiated at 8250 m a.s.l. over the position of the Eyjafjallajökull volcano on 17 April at 19:00 CET. The position of Garmisch-Partenkirchen is marked by a cross.

ACPD
12, 23135–23193, 2012

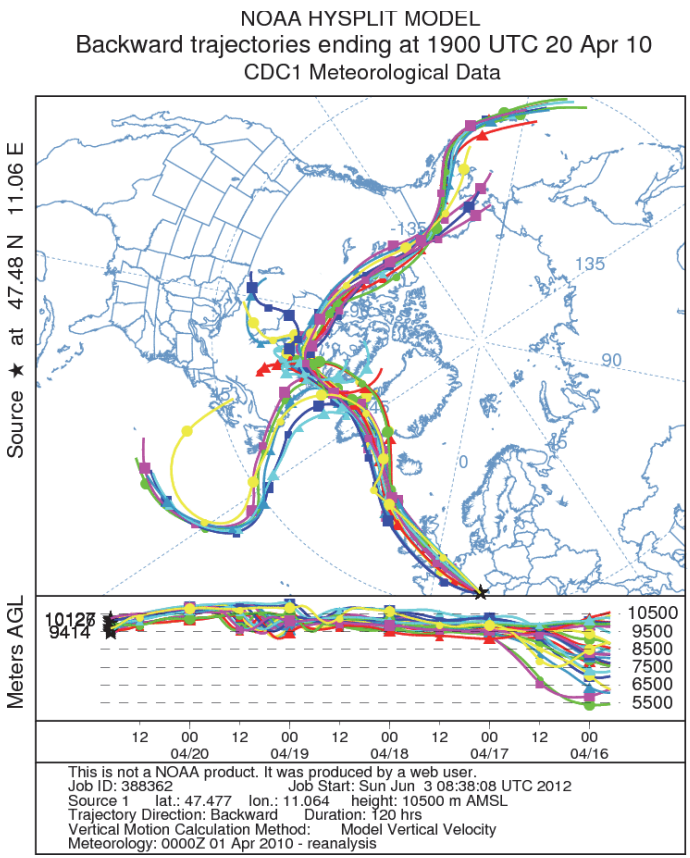

Fig. 16. HYSPLIT backward ensemble trajectories initiated at 10 500 m a.s.l. over the position of IMK-IFU on 20 April at 20:00 CET.

ACPD
12, 23135–23193, 2012

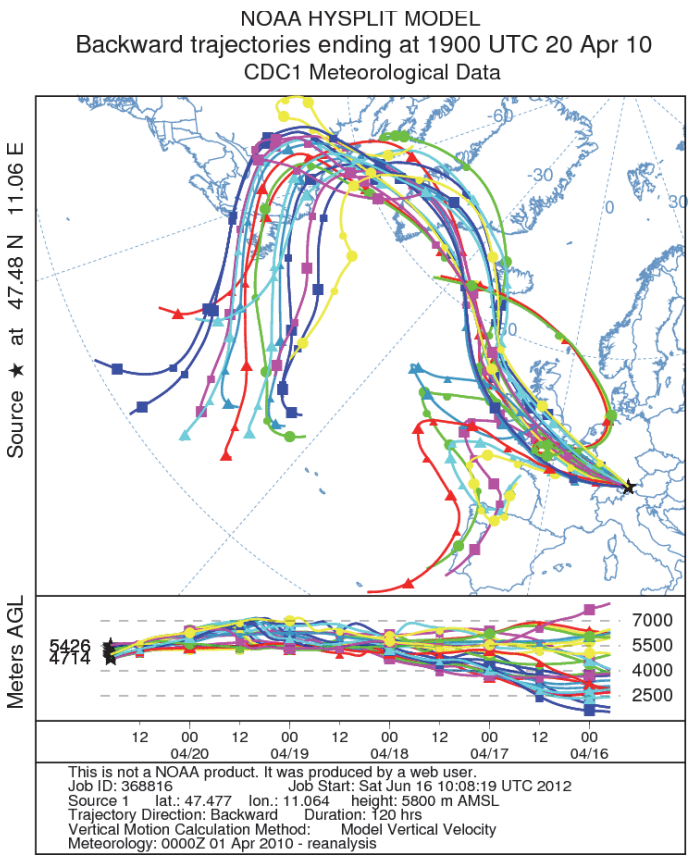

Fig. 17. HYSPLIT backward ensemble trajectories initiated at 5800 m a.s.l. over the position of IMK-IFU on 20 April at 20:00 CET.

ACPD
12, 23135–23193, 2012

Fig. 18. Eruption of Grimsvötn in May 2011; the ash reached an altitude of 20 km (Table 1). Source: dpa Picture-Alliance GmbH.

ACPD
12, 23135–23193, 2012